1   **GO5.0: The joint NERC-Met Office NEMO global ocean model for use in**
2   **coupled and forced applications.**
3
4   Alex Megann[1], Dave Storkey[2], Yevgeny Aksenov[1] Steven Alderson[1], Daley Calvert[2]
5   Tim Graham[2] Patrick Hyder[2], John Siddorn[2] and Bablu Sinha[1]
6
7   [1] Marine Systems Modelling, National Oceanography Centre, Southampton, SO14
8   3ZH, UK
9   [2] Met Office, Hadley Centre, Exeter, Devon, EX1 3PB, UK
10
11   Correspondence to: Alex Megann (apm@noc.ac.uk)

1   **Abstract**. We describe a new Global Ocean standard configuration (GO5.0) at eddy-
2   permitting resolution, developed jointly between the National Oceanography Centre
3   and the Met Office as part of the Joint Ocean Modelling Programme (JOMP), a
4   working group of the UK's National Centre for Ocean Forecasting (NCOF) and part
5   of the Joint Weather and Climate Research Programme (JWCRP). The configuration
6   has been developed with the seamless approach to modelling in mind for ocean
7   modelling across timescales and for a range of applications, from short-range ocean
8   forecasting through seasonal forecasting to climate predictions as well as research use.
9   The configuration has been coupled with sea-ice (GSI5.0), atmosphere (GA5.0) and
10 land-surface (GL5.0) configurations to form a standard coupled global model (GC1).
11 The GO5.0 model will become the basis for the ocean model component of the
12 Forecasting Ocean Assimilation Model, which provides forced short-range
13 forecasting services. The global coupled model (GC1) or future releases of it will be
14 used in coupled short-range ocean forecasting, seasonal forecasting, decadal
15 prediction and for climate prediction as part of the UK Earth System Model.
16
17 A 30-year integration of GO5.0, run with CORE2 surface forcing from 1976 to 2005,
18 is described, and the performance of the model in the final ten years of the integration
19 is evaluated against observations and against a comparable integration of an existing
20 standard configuration, GO1. An additional set of 10-year sensitivity studies, carried
21 out to attribute changes in the model performance to individual changes in the model
22 physics, is also analysed. GO5.0 is found to have substantially reduced subsurface
23 drift above the depth of the thermocline relative to GO1, and also shows a significant
24 improvement in the representation of the annual cycle of surface temperature and
25 mixed-layer depth.
26
27

1   Introduction

Coupled climate models developed at the UK Met Office have been at the forefront of international climate research and projections for the past fifteen years. HadCM3 (Gordon et al. 2000) was used in the Third and Fourth Assessment Reports (Houghton et al. 2001; Solomon et al. 2007) and is still widely used as a standard tool in climate research, while HadGEM1 (Johns et al., 2006), HadGEM2 (Collins et al., 2008) and HadGEM3 (Hewitt et al., 2011) have offered improvements in resolution, numerics and physics. All these models have an ocean on a horizontal grid of around 1°, although the HadGEM models have a refinement of the north-south grid scale close to the Equator down to 1/3°. In this paper we will refer to the model described by Hewitt et al. (2011) as HadGEM3, however newer versions currently in development, with a higher resolution ocean, are also commonly referred to as HadGEM3.

Global ocean models are also used at the Met Office as part of seasonal and decadal forecasting systems (Arribas et al., 2011, Smith et al., 2007) and for ocean analysis and short-range forecasting (Storkey et al, 2010). At the Met Office and elsewhere there is increasing interest in using a seamless modelling system for use at all timescales from short range forecasting to climate prediction (Brown et al 2012).

Increased horizontal resolution in the ocean has been shown to have several benefits for modelling climate. In the North Atlantic the improved path of the Gulf Stream and North Atlantic Current reduces the magnitude of a large cold bias off Grand Banks seen in many low-resolution climate models (e.g. Gnanadesikan et al., 2007; Danabasoglu et al., 2010). Reducing this bias has been shown to improve the frequency of blocking in a climate model (Scaife et al., 2011). In the tropical Pacific ocean, eddy permitting resolution in HiGEM has been shown to help reduce the equatorial cold tongue bias (Shaffrey et al., 2009, Roberts et al., 2009) and the double intertropical convergence zone (ITCZ) bias, and also to more realistically simulate the westward extent of El Niño. Furthermore, teleconnections to the North Pacific Ocean associated with ENSO were also improved as a result of increased ocean resolution (Dawson et al., 2012). Eddy permitting models have an order of magnitude more eddy kinetic energy (EKE) than low-resolution models (Delworth, 2012) and ORCA025

1   has been shown to simulate 81% of observed sea level variability on interannual

2   timescales (Penduff et al., 2010).

3

4   Ocean models run on horizontal grids fine enough to resolve eddies in the Southern

5   Ocean show "eddy saturation", where increased vertical transport of momentum and

6   meridional transport of heat away from the Antarctic Circumpolar Current (ACC) by

7   the eddy field in response to increases in wind stress mean that the isopycnal slopes

8   and therefore the circumpolar transport is relatively insensitive to changes in the wind

9   forcing (Tansley and Marshall, 2001; Hallberg and Gnanadesikan, 2006. Munday et

10   al, 2013). This is not observed in lower resolution models where the eddy transports

11   are parameterised by diffusive schemes. A similar insensitivity of the global

12   overturning circulation to the Southern Ocean wind forcing ("eddy compensation") is

13   also seen in eddy-resolving models (Viebahn and Eden, 2010, Farneti et al, 2010)

14   although some studies have suggested that eddy-compensation can be achieved in

15   lower resolution models using a variable Gent-McWilliams coefficient and modified

16   tapering scheme at the base of the mixed layer (Gent and Danabasoglu, 2011; Farneti

17   and Gent, 2011).

18

19   Here we describe a new Global Ocean standard configuration (GO5.0) at eddy-

20   permitting resolution, developed jointly between the National Oceanography Centre

21   and the Met Office as part of the Joint Ocean Modelling Programme (JOMP), a

22   working group of the UK's National Centre for Ocean Forecasting (NCOF) and part

23   of the Joint Weather and Climate Research Programme (JWCRP). The configuration

24   has been developed with the seamless approach to modelling in mind and is therefore

25   intended to be used as the basis for ocean modelling across timescales and for a range

26   of applications, from short-range ocean forecasting, through seasonal forecasting, to

27   climate predictions as well as research use. The configuration has been developed for

28   use throughout the UK academic and operational modelling communities. It has been

29   coupled with the sea-ice (GSI5.0), the atmosphere (GA5.0) and the land-surface

30   (GL5.0) configurations to form a standard coupled global model (GC1). Additionally

31   we take this opportunity to improve upon known deficiencies in the vertical mixing

32   scheme and to take advantage of recent releases of NEMO and improvements in

33   bathymetry datasets. The GO5.0 model will become the basis for the ocean model

component of the Forecasting Ocean Assimilation Model (FOAM, Storkey et al., 2010), which presently provides forced short-range forecasting services to MyOcean (www.myocean.eu) and other users. The global coupled model will be used in coupled short-range ocean forecasting (as future versions of FOAM evolve into coupled systems), for seasonal forecasting as part of the GloSea4 system (Arribas et al., 2011), for decadal prediction as part of the DePreSys system (Smith et al., 2007) and for climate prediction as part of the UK Earth System Model UKESM. The latter will be the UK's contribution to the upcoming IPCC Sixth Assessment Report and to the Coupled Model Intercomparison Project Phase 6 (CMIP6).

We use the term "standard configuration" to denote all the items required to run the model, i.e. model code, input parameters and datasets, and compilation keys, and these are summarised in the Appendices.

The main aim of this paper is to introduce the ocean model constituting GO5.0, and to evaluate its performance in ocean-only configuration, according to a set of first-order metrics. We will also compare the performance of GO5.0 with the previous global ocean configuration, which we denote GO1, and attribute the salient differences between the two model implementations to specific changes in model physics and parameter sets. Documentation of the attribution of changes in model behaviour to specific choices in a configuration will allow model developers using this or other models to make informed decisions and interpret model simulations with more clarity. Section 2 describes the ocean and ice models and the surface forcing fields. Section 3 summarises the main physics choices, and in Section 4 the experimental design is described. In Section 5 we present the results of the analysis: firstly the GO5.0 configuration is validated against observations; then GO5.0 is compared with the previous global model GO1; and the main improvements identified in GO5.0 are attributed to specific physics choices. Finally in Section 6 we summarise the results and discuss upgrades to the model currently under development.

2   Model description

GO5.0 is based on version 3.4 (v3.4) of NEMO (Nucleus for European Models of the Ocean) (Madec, 2008), and is closely related to the global DRAKKAR ORCA025 configuration (Barnier et al, 2006) sharing many of the same dynamics and physics choices. The horizontal grid, known as ORCA025, has 1/4° resolution (1442 × 1021 grid points) at global scale decreasing poleward (an isotropic Mercator grid in the southern hemisphere, matched to a quasi-isotropic bipolar grid in the northern hemisphere with poles at 107°W and 73°E). The effective resolution is approximately 27.75 km at the equator, but increases with latitude to be, for example, 13.8 km at 60°S or 60°N. The model has 75 vertical levels where the level thickness is a double tanh function of depth such that the level spacing increases from 1 m near the surface to 200 m at 6000 m (Culverwell 2009). This level set was chosen to provide high resolution near the surface for short to mid range forecasting purposes while retaining reasonable resolution at mid-depths for long term climate studies.

The model bathymetry (DRAKKAR v3.3) is based on the ETOPO1 dataset (Amante and Eakins, 2009) with additional data in coastal regions from GEBCO (IOC, 2008). This is a change from the GO1 configuration, which used the DRAKKAR G70 bathymetry based on the lower-resolution ETOPO2 with corrections from satellite-based bathymetry and other sources (Remy et al., 2003). Bottom topography is represented as partial steps (Barnier et al., 2006). The derivation of DRAKKAR bathymetry datasets is described by Barnier et al. (2006). Initially, each model grid cell is assigned the median of all observations falling within the boundaries of that grid cell. The initial estimate is then modified by application of two passes of a uniform Shapiro filter and, finally, hand editing is performed in a few key areas.

The model uses a linear free surface and an energy and enstrophy conserving momentum advection scheme. The horizontal viscosity is bilaplacian with a value of 1.5×10^{11} m^4/s at the equator, reducing polewards as the cube of the maximum grid cell dimension: thus at 60°N the horizontal viscosity is approximately 1/8 of its value at the Equator. Tracer advection uses a Total Variance Dissipation (TVD) scheme (Zalesak 1979). Lateral tracer mixing is along isoneutral surfaces with a coefficient of 300 m^2/s. The isopycnal mixing scheme of Gent and McWilliams (1990) is not used in this configuration.

1

2   With regard to diapycnal mixing processes, the vertical mixing of tracers and

3   momentum is parameterised using a modified version of the Gaspar et al. (1990)

4   Turbulent Kinetic Energy (TKE) scheme (Madec, 2008). Unresolved vertical mixing

5   processes are represented by a background vertical eddy diffusivity of 1.2×10^{-5}

6   m^2s^{-1}, which decreases linearly from ±15° latitude to a value of 1.2×10^{-6} m^2s^{-1} at ±5°

7   latitude (Gregg et al., 2003) and a globally constant background viscosity of 1.2×10^{-4}

8    $m^2s^{-1.}$ A parameterisation of double diffusive mixing is included at GO5.0 (Merryfield

9   et al, 1999).

10   Bottom friction is quadratic with an increased coefficient in the Indonesian

11   Throughflow, Denmark Strait and Bab al Mandab regions. An advective and diffusive

12   bottom boundary layer scheme is included (Beckmann and Doescher, 1997). The tidal

13   mixing parameterisation of Simmons et al. (2004) is included with a special

14   formulation for the Indonesian Throughflow (Koch-Larrouy et al., 2008). At GO5.0 a

15   climatological geothermal heat flux (Stein and Stein, 1992) is added as a bottom

16   boundary condition; this was not used at GO1.

17   The sea ice component is the latest public release of the Los Alamos National

18   Laboratory sea ice model CICE version 4.1 (v4.1, Hunke and Lipscomb, 2010). The

19   model includes Elastic-Viscous-Plastic ice dynamics (Hunke and Dukowicz, 1997),

20   energy-conserving thermodynamics (Bitz and Lipscomb, 1999) and multi-category

21   ice thickness (Bitz, et al., 2001). The setup of CICE is the same as in the lower-

22   resolution version of HadGEM3 described by Hewitt et al. (2011) with five sea ice

23   thickness categories. Both GO5.0 and HadGEM3 use the zero-layer Semtner

24   thermodynamics scheme (Semtner, 1976). We also note that in both the GO5.0 and

25   HadGEM3 configurations the sea ice model is not on the same grid as the ocean (sea

26   ice is on the Arakawa B-grid and ocean is on the Arakawa C-grid; Arakawa, 1966)

27   and an interpolation routine is used to couple these model components. As in

28   HadGEM3, the ice and ocean components are combined into a single executable, so

29   there is no need for a coupler.

30

We shall also discuss the preceding version of the Met Office ocean model, GO1. This was based on NEMO version 3.2 (v3.2) and CICE v4.1, and was implemented on the same grid as GO5.0, with the same surface forcing.

The ocean and ice code are managed using the Subversion code-management software, allowing unique identification of the respective code bases using a code version number. Ocean and Ice model code version numbers, compilation keys and namelists are listed in the Appendices.

The model was run on the MonSOON supercomputer, jointly owned by NERC and the Met Office. The ocean was distributed over 480 cores with the MPI communications harness, with CICE running on a single node, and an acceptable throughput of one model year in six hours was achieved.

3   Summary of main physics choices

The main physics change between GO1 and GO5.0 is a set of changes to the vertical mixing parameters based on the work of Calvert and Siddorn (2013). Vertical mixing in the model is achieved using a turbulent closure scheme with an algebraic mixing length (Gaspar et al., 1990; Madec, 2008). Additionally, the NEMO implementation of the scheme includes a number of parameterisations to represent additional unresolved turbulent processes, including surface wave breaking (Craig and Banner, 1994) and Langmuir turbulence (Axell, 2002). A further parameterisation represents the enhanced mixing due to breaking of near-inertial waves as an additional source of TKE exponentially decaying from the surface. Users of previous versions of the NEMO ORCA025 model have found significant biases, particularly in the mid-latitudes, and this has been highlighted as a priority bias to reduce with this configuration. Calvert and Siddorn (2013) explored the sensitivity of the model to realistic ranges of parameters in the TKE scheme using 10-year integrations of NEMO at ORCA1 (1°) lateral resolution. As a result of this work they found that altering the vertical length scale for this TKE source term (controlled by the parameter *nn_htau*) from 30m to 10m at mid to high latitudes and from 0.5m to 10m

in the tropics was able to significantly alleviate an excessively diffuse mid-latitude thermocline. This was seen to result in reduced summer time mixed layer depths and a significant reduction of near-surface temperature biases at midlatitudes. Additionally, Calvert and Siddorn (2013) suggested that a small increase in the Craig and Banner (1994) wind-wave energy coefficient (controlled by the parameter *rn_ebb*) would be more consistent with theory, but was shown to have a very small impact on model results. Similarly, a minor change in the minimum permitted surface mixing length (controlled by the parameter *rn_mxl0*) suggested by Calvert and Siddorn (2013) for consistency with other vertical mixing parameters was shown to have a negligible impact.

Convection in the model is parameterised as an enhanced vertical diffusivity of 10 m^2s^{-1} for momentum and tracer fields where the water column is unstable. At NEMO v3.2 this enhanced vertical diffusivity was erroneously used in the prognostic equation for the TKE, instead of the vertical diffusivity calculated by the TKE scheme. This was shown to result in a deep bias in wintertime mixed layer depths owing to the non-conservative increase in the calculated TKE. This has since been addressed at NEMO v3.4 and therefore constitutes another difference between GO5.0 and GO1.

Other changes between GO1 and GO5.0 are: changes to other vertical mixing parameters between GO1 and GO5.0 as noted in Table 1; the inclusion of a double diffusive mixing parameterisation at GO5.0; the addition of the bottom boundary layer scheme of Beckmann and Doescher (1997); and the inclusion of a climatological geothermal heating parameterisation at GO5.0.

The inclusion of the particular new processes and parameter choices described above is based on a mixture of recommendations from the recent literature (from low resolution model studies), and on changes considered desirable on strong theoretical or observational grounds.

4   Experimental design

1

2 The GO5.0 configuration can be viewed as a set of incremental changes in the model

3 physics relative to the GO1 configuration. In order to evaluate the GO5.0

4 configuration and to understand the model improvements over GO1, a series of forced

5 ocean-sea ice integrations was performed to assess the effects of each individual

6 change.

7 4.1 Model initialisation and forcing

8 All of the integrations described here are driven over the period 1976–2005 by the

9 CORE2 surface forcing data set (Large and Yeager, 2004). CORE2 supplies monthly

10 precipitation and daily downward shortwave and longwave radiation which are used

11 to force the model directly, and 6-hourly 10 m wind, 2 m air humidity and 2 m air

12 temperature which are used to compute turbulent air/sea and air/sea ice fluxes during

13 model integration using the bulk formulae proposed by Large and Yeager (2004). The

14 source data for precipitation and radiative fluxes are only available from 1979 and

15 1984 onward, respectively. Prior to these dates the respective climatologies are used.

16 Climatological monthly runoffs derived from the Dai and Trenberth, 2002

17 climatology are applied along the land mask (Bourdalle-Badie and Treguier 2006). No

18 diurnal cycle is imposed in the radiative forcing.

19 Initial conditions for temperature and salinity for all the integrations are obtained from

20 an average of years 2004-2008 of the EN3 monthly objective analysis (Ingleby and

21 Huddleston, 2007) and the model is started from a state of rest. To avoid unacceptable

22 drifts in salinity and an excessive spin-down of the overturning circulation, the sea

23 surface salinity (SSS) is restored toward monthly mean climatological values: the

24 vertical velocity for restoration *rn_deds* is set to -33.33 mm day^{-1} psu^{-1} over the open

25 ocean, and a factor of 5 larger under sea ice. Model outputs are archived as successive

26 5-day means throughout the whole integration and post-processed to monthly means.

27 More details about the model configuration may be found in Storkey et al. (2010),

28 Barnier et al. (2006) and Penduff et al. (2007).

29

30 4.2 Model integrations

31

A thirty-year integration of GO5.0 was carried out with the final set of modifications and parameter values, from the initial state described above. This was compared with the reference integration, from the same initial state and of the same length, of the pre-existing GO1 model based on NEMO v3.2. To estimate the effect of the code change alone, a further thirty-year integration of NEMO 3.4 was made with initial state and all parameters and physics choices identical, or as close as possible, to those of GO1. We compare annual and seasonal means from each of these three integrations and also with observations in the form of the EN3 climatology for subsurface temperature and salinity (Ingleby and Huddleston, 2007), the HadSST3 surface temperature climatology (Kennedy et al., 2011), satellite-derived sea-ice extent (Cavalieri, 1996, updated 2013), the PIOMAS reanalysis for Northern Hemisphere sea ice volume (Zhang et al, 2003), and measured transports through key straits from a variety of observational studies.

An additional set of ten-year simulations was made to attribute changes between GO1 and GO5.0 to individual changes in configuration. These are summarised as follows:

- The bathymetry was upgraded from the original Drakkar ORCA025 dataset as described in Section 2;

- The background vertical diffusivity *rn_avt0* and viscosity *rn_avm0* were increased from 1.0×10^{-5} to 1.2×10^{-5} m^{2}s^{-1} and from 1.0×10^{-4} to 1.2×10^{-4} m^{2}s^{-1}, respectively;

- Changes were made to the TKE scheme parameters *rn_ebb* (coefficient of the surface input of TKE), *rn_mxl0* (minimum surface mixing length scale) and *nn_htau* (changing the TKE penetration depth scale from a constant 10 m to varying from 0.5m at the equator to 30m poleward of 40°N and 40°S);

- Geothermal heat flux was applied, as in Stein and Stein (1992) via the parameter *nn_geoflx*;

- Double diffusion of tracers was added;

- A scheme for a bottom boundary layer as in Beckmann and Doescher, 1997 was added;

- The ice model (CICE) was modified to include a salinity-dependent freezing point. The thermal conductivity of the ice was changed from 2.00 to 2.63 W

m^{-1} K^{-1} and the fixed ice salinity was changed from 4.0 to 8.0 psu, following Rae et al (2013).

The attribution study will compare the above experiments with one another, as well as with the v3.2 model GO1 and the original v3.4 integration with the GO1 parameter set. The strategy of adjusting parameters according to individual sensitivity studies may not be the optimal method for finding the most appropriate parameter set, since the parameters and physics choices may interact nonlinearly, but resources were insufficient for a systematic investigation of parameter space such as that carried out with HadCM3 by Williamson et al. (2013).

Table 2 summarises the integrations carried out, including the values of the principal parameter changes at each step.

We note that the pair of runs comparing NEMO 3.2 and 3.4 (namely GO1 and N3.4) differ further in one minor respect. The v3.4 parameter *rn_mxl0*, the minimum permitted surface mixing length, was erroneously set to 0.001 in the latter experiment to match the value of the parameter *rn_lmin* in v3.2. The latter is an interior minimum length scale in v3.2 but is absent in v3.4, and the equivalent parameter in v3.2 is in fact *rn_lmin0*, which was set to 0.01. An additional ten-year integration (N3.4_*mxl0*) similar to N3.4 was performed, with a value of 0.01: the consequent surface changes were not considered to be significant, with the two simulations being qualitatively the same, with mean surface temperature differences in years 6–10 less than 0.05°C everywhere.

5   Results

5.1   Validation of GO5.0 against observations

5.1.1 Surface biases and mixed layer depth

Figure 1 shows the surface temperature (SST) and salinity (SSS) errors in years 21-30 of the GO5.0 model, relative to the mean of the Reynolds et al (2002) and EN3

1 (Ingleby and Huddleston, 2007) respective monthly climatology over the same period.

2 There is overall a warm bias over most of the global ocean, with a global mean bias of

3 +0.72°C, and with the largest biases (of over 1°C) in the tropics, the Southern Ocean,

4 the subpolar North Atlantic and over the separated western boundary currents in the

5 North Atlantic and North Pacific. There are cool biases of 0.25-0.50°C extending over

6 much of the subtropical North Atlantic and North Pacific. GO5.0 is too fresh in most

7 of the Atlantic, except in the subpolar gyre, where the salty bias of 0.5-1.0 PSU is co-

8 located with the warm bias mentioned above. It is worth noting that the largest surface

9 errors occur at high latitudes, and therefore are perhaps unduly emphasised in the

10 cylindrical projection used in Figure 1. Generally the regions where there is a surface

11 warm bias (especially in the Southern Ocean and the Pacific) correspond to a positive

12 surface salinity error: these may result from forcing errors, but are not inconsistent

13 with an excessive evaporation from surface waters with a warm bias. The exception is

14 in the Arctic, where there is a positive surface salinity error of up to 2 psu, due to

15 excessive autumn sea ice formation on the Siberian shelves and in the Beaufort Sea

16 (Fig 1); the reason for this error is unclear, but is most likely to be related to the air

17 temperature and radiative biases in the atmospheric forcing (Barnier et al., 2006). The

18 sea ice biases are discussed further in the section 5.1.4.

19

20 Figure 2 shows the annual minimum and maximum mixed-layer depth (MLD)

21 calculated for years 1996-2005, corresponding to the shallowest depth of the mixed

22 layer in the local hemispheric summer and the deepest mixed layer in the local

23 hemispheric winter, alongside the same quantity from the de Boyer Montégut et al

24 (2004) climatology. The model mixed-layer depth is calculated from 5-day data using

25 the same criterion of a 0.2°C change relative to the surface value as used in the

26 climatology. The ocean data points masked by hatching in the model output (panels a

27 and c) and by white in the climatology (panels b and d) represent the locations where

28 a full annual cycle of observations was not available as a result of sea ice coverage.

29 The GO5.0 model realistically reproduces the spatial patterns of both summer and

30 winter surface mixing: in particular, the regions of wintertime dense water formation

31 in the North Atlantic and Nordic Seas correspond quite closely to those in the

32 observations, as do the near-zonal bands of deep turbulent mixing in the Southern

33 Ocean (Figs 2c, d). There is a consistent bias, however, to an unrealistically shallow

1 summer mixed layer over the whole ocean, with maximum values of 30-50 metres in

2 the tropics and Southern Ocean in the model, contrasting with a range of 50-70 metres

3 in the same regions in the climatology (Figs 2a, b). This is consistent with the warm

4 surface bias in the same regions seen in Figure 1. Also, the winter mixing in the dense

5 water formation regions in the North Atlantic is much deeper than in the climatology,

6 reaching to over 1000 metres in many instances. The patch of very deep mixing

7 extending from the Weddell Sea eastwards to 50°E is also seen in HadGEM1 and

8 HiGEM: in GO5.0 this feature develops after year 20 of the integration, but it does

9 not occur in GO1. It seems to be associated with a gradual modification of the

10 watermasses in the region and the development of the extensive polynya visible in

11 Figure 6(c), which together precondition for the deep mixing, but the exact

12 mechanisms are yet unclear. The simulated deep winter mixed layer in the eastern

13 Weddell Sea in the 1990s and 2000s is likely to be unrealistic, although the limited

14 winter data in the area (e.g., Sirevaag et al., 2010) prevents us from making any

15 definitive conclusion. From the Conductivity Temperature Depth (CTD) data

16 collected using Weddell seals, Årthun et al. (2013) surmised that the maximum MLD

17 in the region of the Antarctic Bottom Water formation in the Southern Weddell Sea is

18 in excess of 500 m, which is consistent with the model results (Fig 2c).

19

20

21 The surface biases of the model when forced by prescribed surface boundary

22 conditions are to a large degree constrained by the forcing fields, but the subsurface

23 drifts are a stronger test of the model, revealing discrepancies in diapycnal mixing and

24 advection pathways. Figure 3 shows the zonal mean temperature and salinity

25 anomalies in GO5.0 averaged from 1996 to 2005, with reference to the EN3

26 climatology. The black contours show the zonal mean potential density σ_0, with a 0.5

27 kg m^3 contour interval, to illustrate the position of the biases with respect to the main

28 pycnocline. The largest biases are in the top 700 metres of the water column: these

29 include a cold subsurface bias (~2°C) around Antarctica; a warm salty bias (~1.5°C

30 and 0.25 psu) between 45 and 60°S; a warm bias in the tropics of up to 2.5°C down to

31 about 200m; cold, fresh biases in the main thermocline (45°S-45°N, with maximum

32 discrepancies of 1°C and 0.5 psu); and a warm salty bias in the northern hemisphere

33 subpolar gyre regions (~1°C, 0.25 psu).

1

2   5.1.2 Atlantic Meridional Overturning

3

4   Figure 4(a) shows a time series of the North Atlantic overturning strength at 26°N for

5   the full 30-year integration of GO5.0, alongside that in GO1. Also shown is the

6   potential density averaged over the upper 200 m in the central Labrador Sea (55°-

7   58°N, 48°-50°W). Figure 4(b) illustrates the meridional overturning streamfunction in

8   years 1996 to 2005 in both models. In both GO1 and GO5.0 the overturning

9   circulation reaches a maximum in the second decade of the integration, reducing by 2-

10   3 Sv by year 30; the run length is however not sufficient to determine whether the

11   circulation has settled at that stage. In both runs both the MOC and the Labrador Sea

12   density increase over the first decade and decrease later in the second decade,

13   consistent with the hypothesis that the Labrador Sea surface density controls the

14   overturning, although a longer time series would be required to establish a statistically

15   robust correlation. The overturning strength at 26°N in the final decade is between 21

16   and 22 Sv, which is significantly stronger than the value of 18.5±1 Sv observed

17   between 2004 and 2008 by the RAPID WATCH/MOCHA array (McCarthy et al

18   2012). Interestingly, the downward trend we see in the last decade of the model runs

19   (~2-3 Sv/decade) is similar to that recently reported from the RAPID array (Smeed et

20   al 2013). The modelled annual means for two years overlapping the observations,

21   namely 2004 (19 Sv) and 2005 (20 Sv) match well with the observations (17.8 Sv and

22   20.1 Sv respectively), and the strength of the modelled AMOC over the latter decade

23   of the run is entirely plausible, particularly since recent studies indicate that a

24   substantial fraction of the variability in the strength of the AMOC originates from

25   surface forcing (Roberts et al 2013, Blaker et al 2013). We cannot expect the model to

26   simulate the measured AMOC perfectly, since a significant fraction of the AMOC

27   variability is inherently unpredictable, arising as a consequence of baroclinic wave

28   field and mesoscale eddy field (Hirschi et al 2013, Thomas and Zhai, 2013). Hirschi

29   et al., (2013), performed forced 1/4° simulations similar to those described in this

30   paper with different initial conditions: in the simulations of Hirschi et al about 70% of

31   the AMOC variability is determined by the surface forcing, and 30% from intrinsic

32   ocean variability. We expect this to be an underestimate, since our model

33   configuration is eddy permitting, rather than eddy-resolving. The question of the

physical processes contributing to AMOC variability in models and observations (for example, Ekman transport, advection of density anomalies and Rossby waves) is complex and has been explored in a number of recent papers (e.g. Sinha et al., 2013, Roberts et al., 2013, Robson et al., 2014), but is beyond the scope of the current paper. We note that the modelled annual means quoted here are Jan-Dec, whilst the observational array figures are April-March.

Figure 4(b) also shows that the depth of the North Atlantic Deep Water (NADW) return flow is too shallow. At 26ºN the depth of the NADW return flow (usually defined as the depth of the zero contour in the streamfunction) is around 3,500m for most of the model run compared to deeper than 4,000m in the RAPID array data. This is a common bias in many ocean GCMs using depth coordinates, and is usually attributed to spurious mixing of overflow waters as they descend from passages in the Greenland-Iceland-Scotland ridges to the deep ocean (Saunders et al., 2008, Danabasoglu, 2010). It is worth noting that substantial variation in the depth profile can arise from the method used to compute the overturning. Computing the overturning from a model using the RAPID array methodology and assuming a geostrophic reference depth of 4,740 m can yield a transport profile much more similar to the observations at 26°N than integrating the model velocities (Roberts et al, 2013).

The increase in the AMOC over the first decade of the model run is a phenomenon often seen in ocean GCMs using mixed surface boundary conditions in which the high latitude oceans become overly sensitive to salinity perturbations (Rahmstorf and Willebrand, 1995; Lohmann et al., 1996, Greatbach and Peterson, 1996; Griffies et al., 2009; Yeager & Jochum, 2009). In the GO5.0 model run an initial error in the path of the North Atlantic Current (NAC) causes warm, salty water to be advected into the subpolar gyre where it joins the Greenland current and enters the Labrador Sea. The prescribed surface air temperature causes excessive surface heat loss in the Labrador Sea, increasing the density of the surface waters and leading to excessive deep water formation in this region. The increase in the MOC causes more warm, salty water to be advected into the subpolar gyre in a positive feedback. Yeager and Jochum (2009) show that stronger sea surface salinity restoring can reduce this

1 feedback mechanism by reducing the surface salinity in the Labrador Sea. This

2 improvement, however, comes at the expense of realistic interannual variability in the

3 global climate.

4

5 5.1.3 Critical sill and strait transports

6

7 Table 3 lists the volume transports through the major straits and across critical sills,

8 evaluated from the model velocities averaged over the last 10 years of the 30-year

9 integrations of GO1 and GO5.0, together with recent observed estimates and their

10 sources. The sign convention is positive for northward and eastward flow. Overall, the

11 models simulate these transports acceptably: in particular, the Drake Passage

12 throughflow is much closer to observations than those in the lower-resolution coupled

13 models HadCM3 and HadGEM1, both of which at ~200 Sv (Johns et al., 2006) are

14 unrealistically strong. HadGEM2 (Collins et al., 2008) gave a comparable simulated

15 Drake Passage transport of ~140 Sv (Meiers et al., 2012). In contrast to these

16 aforementioned coupled models, the 1/4° resolution of the ORCA025 grid allows the

17 present model to at least approach an explicit resolution of the narrower passages: in

18 particular, it can be seen that both GO1 and GO5.0 have transports through the Bering

19 Strait of well within a factor of two of the observed values.

20

21 The Indonesian Throughflow is too strong in both GO1 and GO5.0, which may be due

22 to insufficient enhancement of the tidal mixing in this region (Koch-Larrouy et al.,

23 2008).

24

25 Comparing the model-derived and observation-based estimates of the Arctic-Atlantic

26 exchanges across the Greenland-Scotland Ridge, through Fram and Davis Straits, and

27 through the Barents Sea shows that in both 30-yr model runs the volume transports

28 are within 10-20% of the long-term mean observed values and within the range of the

29 observational uncertainties, except for the Denmark Strait overflow where the model

30 estimates are 33% (GO1) and 45% (GO5.0) higher than the observational estimate

31 (Table 3). Although the simulated net outflow from the Arctic Ocean, of 4.8 Sv in

32 GO1 and 4.6 Sv in GO5.0, is very close to the observed value of 4.6 Sv, the model

33 shows a different partitioning of the exports west and east of Greenland: the simulated

flow through the Canadian Archipelago is larger than the export through Fram Strait, which is opposite to the observations. The bias is stronger in summer than in winter and is due to excessive Ekman convergence in the Beaufort Sea; this in its turn is caused by the summer sea ice extent being too low (see next section). The simulated Pacific inflow in Bering Strait is higher than in the observations, even considering the recent update in the latter estimate (Woodgate et al., 2012). The simulated northward ocean velocities in the strait are about 35% higher then those observed at the long-term moorings (Clement Kinney et al, 2014). Aagaard et al (2006) suggested that the flow through the Bering Strait is partly driven by the local wind and partly by the steric height difference between the Bering and Chukchi Seas. The latter is caused by the fresher, warmer waters been present to the south of the strait and colder, more saline waters to the north of the strait (Aagaard et al., 2006). In the model the positive bias in salinity in the Chukchi Sea and the Eastern Arctic (Fig 1b) increases the steric height gradient from the North Pacific to the Arctic Ocean, increasing the northward flow through the Bering Strait. The stronger Pacific inflow brings extra heat in the Arctic Ocean, which may contribute to the excessive sea ice melting.

Overall, both runs, GO1 and GO5.0, present more vigorous northward flow of the Atlantic water than is observed ("Total Greenland-Scotland inflow" in Table 3 is a proxy for this) and stronger than observed return overflows across the Greenland Scotland Ridge: the combined overflows in Denmark Strait and in the opening between Iceland and the Faeroes and between the Faeroes and Scotland are 6.3 Sv from the data, 9.3 Sv in GO1 and 8.3 Sv in GO5.0. This is also evident in the stronger simulated AMOC compared to observations.

It should be noted that the observational estimates of the exchange transports into and out of the Arctic should be treated with caution. First, in all straits, except for the moorings in Bering Strait, the hydrographic section in Fram Strait and the one in the Barents Sea between Norway and the Bjørnøya (Barents Sea Opening), uninterrupted records from current meter moorings are no longer than two years. This aliases interannual variations and introduces large uncertainties in the observational transports estimates. Secondly, the instruments were not positioned in the top 50 m or on shallow shelves, in order to prevent the moorings being damaged by sea ice keels.

1   Lastly, the distances between the moorings were too great to resolve mesoscale

2   variability of the flows and in Bering Strait the transports were derived from velocity

3   measurements obtained from three separate moorings (e.g., Woodgate et al., 2012).

4   All this introduces spatial aliasing in the interpolating procedures and uncertainties in

5   the transports. For detailed discussion of uncertainties in observed transports, please

6   refer to e.g. Curry et al., 2011 and Olsen et al., 2008. It also should be noted that,

7   while the model standard deviations in the table represent variability of the transports

8   on synoptic to interannual timescales, the standard deviations of the observational

9   estimates include uncertainty inherent in the estimation methods as well as the

10   variability of the transports, thus rigorous comparison of the variability in the model

11   and data requires additional analysis, not presented here.

12

13   5.1.4 Sea ice

14

15   In Figure 5 timeseries of the sea ice extent and ice concentration in the Northern and

16   Southern hemispheres are compared with products from passive microwave satellites

17   SSMR/I and AVHRR (Cavalieri, 1996, updated 2013). In the Northern Hemisphere

18   the simulated annual mean of 11.2×10^6 km^2 and the amplitude of the seasonal cycle

19   of 7×10^6 km^2 are in good agreement with the data (12.4×10^6 km^2 and 5.8×10^6 km^2,

20   respectively), suggesting good model skill in simulating sea ice extent (Figure 5(a)),

21   although the model underestimates summer sea ice extent. The simulated and

22   observed interannual trends also agree. Figure 5(b) compares the modelled Arctic sea

23   ice volumes with these derived from the PIOMAS reanalysis (Zhang et al., 2003).

24   Simulated sea ice volumes are about 60% of those observed through the annual cycle,

25   with winter (DJF) biases of around 30% and in summer (JJA) of around 50%. Despite

26   this bias, the multidecadal trends in the modelled and observed sea ice extents are

27   comparable, showing sea ice extent decline at a rate of -44 $\times 10^3$ km^2 per year and -45

28   $\times 10^3$ km^2 per year, respectively. In the Southern Hemisphere the modelled sea ice

29   extent is again in good agreement with observations (Figure 5(c)), but with a

30   moderate negative summer bias. At present no published sea ice volume timeseries

31   are available for Antarctica, rendering formal validation of the model skills in

32   simulating sea ice volumes in the Southern Hemisphere impossible. However,

33   comparing simulated sea ice thicknesses around Antarctica for 1996-2005 with the

34   Antarctic Sea Ice Processes and Climate (ASPeCt) data (Worby et al., 2008) for the

same period, we conclude that the simulations underestimate long-term mean annual sea ice thickness by about 22% (0.76 m in the model and 0.89 m for simulations and data respectively). The annual cycle in the model is in good agreement with the observations, with the maximum ice thickness (1.06 m and in the model and 1.02 m in the observations) occurring in the austral summer (DJF) and minimum ice thickness (0.58 m in the model and 0.60 m in the observations) in the austral winter (JJA). The simulated sea ice extent trend in the Southern Hemisphere is negative and around -58 x 10^3 km^2/year, in contrast to the positive trend of 13 x 10^3 km^2/year in the observations. The negative trend in Antarctic sea ice extent is a common feature of global ocean models, and is attributed by Holland and Kwok (2012) to biases in the surface winds around Antarctica in the forcing data.

Comparison between the simulated sea ice concentration fields and those from the HadISST observational dataset (Rayner et al., 2002) show that the simulated winter sea ice distribution in both hemispheres is realistic (Figure 6a, b, c, d), although we note that there is a tongue of reduced ice cover extending eastward from the central Weddell Sea, which has also been seen in HadGEM1 and the higher-resolution HiGEM (Shaffrey et al., 2009), and which corresponds to the very deep winter mixing described in Section 5.1.1. The summer sea ice concentration in the model is lower than in the data (e, f, g, h). In the Arctic Ocean this is likely to be caused by the negative bias in the sea ice thickness, which in turn results in lower ice strength, faster ice drift toward the Canadian Arctic Archipelago and thus increased divergence of sea ice in the Central Arctic Ocean. This, combined with the increased sea ice melting in summer due to exposure of the ocean surface to the atmospheric heat, could sustain the lower thicknesses in the Arctic throughout the year. In the present forced simulations, the summer sea ice bias primarily affects polar regions and has a moderate effect on the global ocean circulation. However, in a fully coupled model atmospheric dynamics might cause a significant effect on regions remote from the ice-covered oceans.

5.2   Comparison of GO1 and GO5.0

As shown in Figure 1, GO5.0 shows large-scale surface biases, which are nevertheless not untypical of comparable forced ocean models and are in part due to forcing errors. It is worth noting that the impact on the coupled model of the vertical mixing changes is expected to be greater. We shall show in this section that, while the surface biases in the GO1 configuration are similar in most regions of the ocean to those already described in GO5.0, there are significant improvements in the subsurface drifts and the representation of the annual cycle of surface temperature in GO5.0, both of which are likely to lead to improvements in climate simulations.

5.2.1 Subsurface drifts

Figure 7 shows the global zonal mean temperature and salinity drifts of GO1 and GO5.0, defined as the difference between from the respective mean for each year and the corresponding mean for the first year of integration, from the surface to a depth of 1,000 m. We note that the drifts in both models are an order of magnitude larger that the comparable trends in the EN3 climatology (not shown). The temperature field in the upper 300 metres reaches a quasi-equilibrium state after about five years of integration. Both models warm in the above depth range, with a maximum at about 120 metres depth: in GO1 the maximum is up to 0.6°C, while in GO5.0 the warming at the same depth only reaches 0.3°C. Below 300 m both models cool, with a similar maximum rate at 600 m of around -0.12°C per decade. The salinity, by contrast, does not equilibrate, even in the upper ocean, and both GO1 and GO5.0 freshen globally, with a maximum rate at 200 m of 0.036 psu/decade in the former and 0.025 psu/decade in the latter. We note that the warm error in GO5.0 is mainly in the northwest Atlantic and Southern Ocean, while this model generally is too fresh at the surface, with the exception of the Arctic (where there is a large salty surface bias of 1-2 psu), and the Southern Ocean. There is also interannual variability in the globally averaged surface temperature and salinity in the upper 200 metres: this is not well correlated with that of the surface variability, so is not likely to be a direct signature of the ENSO cycle.

It is interesting to relate the drifts in GO1 and GO5.0 to those over the first thirty years of HadGEM1 (Johns et al, 2006) and in CHIME and HadCM3 (Megann et al.,

2010). All these except for CHIME (which uses a hybrid isopycnic-coordinate ocean, in contrast to the depth-coordinate ocean model in the other three) have a pronounced freshening in the upper ocean that steadily penetrates into the interior, and this is likely to be a consequence of the numerical diapycnal mixing typical of this model type (Griffies et al., 2000). HadCM3 and HadGEM1 (which shared an ocean model, albeit on a slightly different grid) similarly had a negative surface temperature error over most of the ocean, offset in HadCM3 by a warm bias in the Southern Ocean, while CHIME had a warm surface error, consistent with a reduced drawdown of heat by numerical mixing.

5.2.2 Seasonal cycle of surface temperature and mixed layer depth

Figure 8 shows the mean biases of the sea surface temperature in GO1 and GO5.0 with respect to the interannual Reynolds et al climatology in the boreal winter and boreal summer seasons, defined as December/January/February (DJF) and June/July/August (JJA) periods respectively. It is clear that both configurations have substantial biases in the time-averaged surface fields, and as with the 10-year mean fields discussed in Section 5.1.1, in many regions these biases are very similar: for example, the tropics and Southern Ocean are generally too warm in both configurations, while the northern high latitudes are generally too cold, and there is a warm error in the subpolar North Atlantic with maximum values of 3-4°C in the boreal winter. There are regions where the seasonal biases in GO1 are smaller than in GO5.0: for example, the cold boreal winter error in the subtropical North Atlantic is larger in GO5.0 south of the separated Gulf Stream (Figures 8(a) and (b)), and in the Southern Ocean there is a substantial coherent warm error in GO5.0 in the austral summer that is not present to the same extent in GO1. Overall, however, there are large-scale reductions in seasonal bias, particularly in the northern summer (JJA) season: the cold errors in the North Atlantic and North Pacific are substantially reduced in GO5.0, as are the warm biases in the tropics and the Southern Ocean. To quantify the improvements, the global RMS SST error in the boreal summer (JJA) is reduced from 0.93°C in GO1 to 0.65°C in GO5.0, while the global mean boreal winter (DJF) error is reduced from 0.79°C to 0.67°C.

1   To illustrate the latitude dependence of the large-scale seasonal biases in GO1 and

2   GO5.0, Figure 9 shows latitude-time plots of the zonally averaged surface

3   temperature bias (referred to the Reynolds et al climatology) and MLD error (referred

4   to the de Boyer Montegut et al (2004) data) in GO1 and GO5.0. This shows more

5   clearly that the boreal summer warm bias in the tropics is reduced in GO5.0, as is also

6   the large summer cold bias in the northern subtropics. As we have already noted,

7   GO5.0 shows systematic biases in both the minimum and maximum MLD (Figure 2):

8   specifically, in both hemispheres winter mixed layers are generally too deep, while

9   summer mixed layers are generally too shallow. The main difference between GO1

10   and GO5.0 is that mixed layer depths are generally shallower in GO5.0, leading to

11   increased stratification and hence the warmer summer surface temperatures,

12   especially in the Southern Ocean, seen in Figure 8(b) and 9(a). The winter MLD

13   biases, by contrast, are generally reduced in GO5.0.

14

15   5.2.3 Surface heat fluxes

16

17   Although the model uses the CORE2 forcing dataset, the use of bulk formulae to

18   calculate some of the components of the heat flux means that the actual heat input to

19   the ocean will be slightly different from the climatological field, and will reflect the

20   surface temperature biases of the model. Figure 10(a) shows the zonal mean net

21   downward surface heat flux in GO5.0 and GO1, alongside the corresponding mean

22   from the CORE2 dataset, while Figure 10(b) shows the difference in the surface heat

23   flux between the two model configurations. The physics changes between GO1 and

24   GO5.0 can be seen to lead to changes in the heat flux that are generally small

25   compared with the difference between the models and the climatology. In tropical and

26   subtropical latitudes the zonal mean surface flux in both model integrations is within

27   5-10 W m^{-2} of the observations, while the excessive heat loss of up to 20 W m^{-2}

28   between 60°N and 70°N and south of 60°S in both cases may be linked with the warm

29   biases described in Section 5.1.1 in these latitude ranges. The regional differences in

30   heat flux between the model versions correspond closely to differences in surface

31   temperature, with the reduction in the warm bias in the tropical Atlantic and Pacific

32   from GO1 to GO5.0 (visible in Figure 9(a) and (b)) leading to an increase of up to 25

33   W m^{-2} in the heat flux into the ocean in these regions, and similarly the reduction in

wintertime cold bias in subpolar latitudes seen in Figure 9 corresponds to a decreased heat loss over the Labrador Sea. In the Southern Ocean the increased surface flux error is larger in GO5.0 relative in GO1 is linked to the intense Weddell Polynya that develops in in GO5.0.

5.3   Attribution of changes

In this section we refer to the experimental design described in Section 4, where a series of shorter (10-year) integrations are made. The model code is first upgraded from NEMO v3.2 to v3.4, then other changes are progressively made within v3.4, to attribute the most significant changes in model fields to specific changes in the model physics. These changes are summarised in Table 2. We compare the mean fields in the final five years (1981-1985) of each ten-year integration; the main comparison will be of the surface fields, but the global subsurface biases down to 700 m will also be compared. We use an empirical criterion for the significance of the changes, since the variance of the fields discussed here was not available in the model output: we judge a modification to have a negligible effect if it leads only to differences in the 5-year mean field with the characteristic signature of the mesoscale eddy field, while modifications which lead to coherent large-scale changes in temperature or salinity are deemed to have a significant effect.

5.3.1 Correction to TKE convective mixing

The code changes from NEMO version 3.2 to 3.4 have one main physics component: which is the correction to the treatment of convective mixing in the TKE scheme described in section 3. As explained in section 3, the expected change to the solution due to this correction is an improvement in the excessively deep wintertime mixing. Figure 11 shows that the code upgrade clearly has significant effects on the surface fields: there are basin-scale changes over almost the whole ocean, with warming of 0.1-0.2°C over the Arctic and the subtropical gyres, but cooling by a similar magnitude on the equator and coastal upwelling regions, in the Southern Ocean and in the North Atlantic subpolar gyre. The surface salinity changes are also predominantly in zonal bands, with the largest increases of 0.2-0.4 psu between 15°S and 30°S and

1   between 15°N and 30°N in the Atlantic and eastern Pacific and a surface freshening

2   over much of the Southern Ocean. The code change overall, however, has little effect

3   on the RMS surface errors of the model: the RMS SST error reduces from 0.665 to

4   0.657°C, while the RMS surface salinity error barely changes from 0.828 to 0.825

5   psu. There are, however, major subsurface effects resulting from the code upgrade,

6   particularly from the correction to the treatment of convective mixing in the TKE

7   scheme: comparing the temperature changes in the upper 700 metres with the mean

8   isopycnal depths (Figure 12) shows that the upgrade removes much of the warm bias

9   in the thermocline region between 50°S and 60°N, via a mean cooling of up to 1°C in

10 the depth range from 50 to 250 metres over these latitudes. Additionally, the drastic

11 reduction in winter MLD biases between v3.2 and v3.4 observed in Figure 9 can be

12 directly attributed to the convective mixing correction. The crescent shape of the

13 temperature bias with respect to the observations (and of the difference between v3.2

14 and v3.4) in Figure 12 reflects the deepening of the thermocline with increasing

15 latitude.

16

17 5.3.2 TKE parameters

18

19 As a reminder to the reader we note that the main reason for performing this

20 sensitivity test was to investigate the effect of altering the vertical length scale for the

21 TKE source term at 1/4° resolution. In the 1° resolution experiments of Calvert and

22 Siddorn (2013) reducing this length scale in midlatitudes and increasing it in the

23 tropics significantly alleviated an excessively diffuse mid-latitude thermocline,

24 reduced summer time mixed layer depths and significantly reduced near-surface

25 temperature biases at midlatitudes. For consistency with theory, we simultaneously

26 made a small increase in the wind-wave energy coefficient and the minimum

27 permitted surface mixing length (controlled by the parameter *rn_mxl0*) but these are

28 expected to have a negligible impact.

29

30 The changes to the TKE scheme parameters lead to a consistent surface warming of

31 between 0.1 and 0.5°C north of 30°N and south of 30°S (Figure 13), while there is a

32 small cooling of around 0.05°C in the tropics. The pattern of the associated salinity

33 changes is more complex, with freshening of up to 0.2 psu in the Arctic, in the

subpolar North Pacific, and to a lesser extent in the tropics and along the path of the ACC; and an increase in salinity in the subtropical zones and, interestingly, in the regions dominated by the Amazon and Congo river plumes. The subtropical surface warming is balanced by a cooling down to 300 m in these latitudes (Figure 14), consistent with reduced vertical mixing.

We conclude that changing the vertical length scale for the TKE source term has similar beneficial effects at 1/4° resolution as at 1° resolution and therefore recommend making this change to the existing scheme.

5.3.3 Bathymetry and background diffusivity and viscosity

The rationale for upgrading the bathymetry is that the new bathymetry is based on higher resolution data (ETOPO1 instead of ETOPO2) and therefore more accurate. Upgrading the bathymetry (not shown) leads to small changes in the temperature and salinity in the Arctic, which overall cools by 0.05°C or less and freshen by around 0.05 psu: this is likely to be a consequence of minor modifications to the North Atlantic sill topography. There are southwards displacements of the path of the topographically-steered ACC, north of the Kerguelen Plateau and north of the Pacific Antarctic Ridge at 140°-150°W, along with a depression of the surface elevation in the Southern Ocean by 3-5 cm (not shown), which may be associated with alterations in the path and strength of the northward-flowing Antarctic Bottom Water.

The current consensus within the NEMO community is that background diffusivity and viscosity should be of the order of 1.2×10^{-5} m^2s^{-1} and 1.2×10^{-4} m^2s^{-1} respectively and since these increases do not degrade the model simulation we argue that these are appropriate values to employ. Increasing the background vertical diffusivity and viscosity parameters (*rn_avt0* and *rn_avm0* respectively) by 20% (not shown) has a small effect on the surface fields, relative to the other parameter changes. There is a general surface freshening in the Arctic by 0.02-0.04 psu, and a hint of warming north of the ACC, but elsewhere any signal is small compared with the mesoscale noise. In the upper ocean the explicit representation of mixing processes by the TKE scheme, dominates the background term, while it is also likely that over much of the ocean the

1   numerical mixing in the model's advection scheme is at least as large as that

2   associated with the 1.2 x 10^{-5} m^2s^{-1} explicit background diffusivity, as discussed in

3   Griffies et al (2000) and Lee et al (2002).

4

5   We conclude that changing the bathymetry and the background vertical mixing

6   parameters does not result in significant global effects on the solution. However we

7   note that the more realistic bathymetry is likely to be important for local circulation,

8   particularly in the Southern Ocean.

9

10   5.3.4 Geothermal heating, double diffusion, bottom boundary layer and ice model

11   changes

12

13   Geothermal heating and double diffusion are physically present in the real ocean, but

14   on the relatively short time scales discussed in this paper, their effects are expected to

15   be small. Nevertheless, in order to make our model as complete as possible, and

16   bearing in mind potential future applications, we explicitly perform sensitivity

17   experiments to evaluate their significance. The addition of benthic geothermal heat

18   input (not shown) leads to a surface freshening of 0.1-0.2 psu between 40° and 50°S

19   in the southwest Atlantic by the end of the 10-year integration, but little large-scale

20   surface effects elsewhere. Adding double diffusion (also not shown) again has

21   relatively little effect on the surface temperature, apart from a small localised cooling

22   along the path of the ACC by 0.05°C, but does produce a freshening of 0.05 psu over

23   much of the Atlantic and the subtropical Pacific. Neither change was expected to

24   have a large subsurface effect over the time scale discussed here, and this is

25   confirmed by our experiments.

26

27   The rationale for inclusion of the bottom boundary layer scheme was to improve the

28   representation of overflows, which are known to be a weak point of z-coordinate

29   models such as NEMO. The bottom boundary layer scheme leads to a surface cooling

30   of ~0.2°C north of the separated Gulf Stream, while larger modifications of up to 1°C

31   to the temperature are seen near the sea floor in the region downstream of the

32   Denmark Strait overflow, but the relationship of the surface signal to the deep

1   temperature signal and associated changes to the deep western boundary current are

2   complex and require further analysis beyond the scope of the present paper.

3

4   As explained in Section 4, the ice model changes consisted of salinity dependence for

5   the freezing point of water, and increases in ice thermal conductivity and salinity, in

6   line with the latest observations. The addition of salinity dependence is justified on

7   the grounds that it is more realistic, whilst the changes to the ice salinity and thermal

8   conductivity are based on the work of Rae et al (2013) where the ice model

9   parameters were tuned to provide agreement with the observed seasonal cycle of ice

10   extent. The changes to the ice model (not shown) give a surface cooling (of ~0.2°C)

11   and freshening (of ~0.1 psu) in the Southern Ocean and a similar cooling in the

12   Arctic. The change in salinity is consistent with increased salt export from the polar

13   regions (both polar regions are associated with net ice export). The increased thermal

14   conductivity is expected to increase ice formation and overall ice cover and hence to

15   reduce the annual mean surface water temperature (since at a given location there will

16   be a longer ice-covered period annually compared to the previous model

17   configuration, GO1).

18

19   5.3.5 Attribution study summary

20

21   In summary, we find that the largest changes result firstly from the ocean code

22   version upgrade from NEMO v3.2 to v3.4, due to an improvement in handling of

23   diffusion of TKE when convection occurs; and secondly from the changes to the

24   parameters of the TKE scheme: namely, the parameters *rn_ebb*, *rn_mxl0* and *nn_htau*.

25   These have only a small effect on the surface errors, but in combination the two

26   changes result in much more substantial improvement of the subsurface temperature

27   field and the seasonal cycle, as described in Section 5.2.

28

29

30   **6   Summary and discussion**

31

32   We have introduced a new ocean model configuration, GO5.0, developed jointly

33   between the Met Office and NERC. This is an implementation of version 3.4 of the

1   NEMO model, on the ORCA025 grid, with horizontal resolution of at least

2    $^1/_4°$ everywhere, together with the CICE sea ice model on the same grid. The GO5.0

3   model configuration is derived from the previous GO1 through an upgrade of the

4   NEMO code version from version 3.2, and a set of parameter changes. A 30-year

5   integration of GO5.0, run with CORE2 surface forcing from 1976 to 2005, has been

6   compared with GO1 with the same forcing. We have additionally described a set of

7   10-year sensitivity studies carried out to attribute changes in the model performance

8   to individual changes in the model physics.

9

10   The GO5.0 configuration was validated against observations during the final ten years

11   of the 30-year integration. It was found to have a generally warm surface bias, with

12   respect to the EN3 climatological dataset, of 0.5°-1°C in the tropics, a cool bias of

13   similar magnitude in the extra-tropics and a warm bias of around 2°C in much of the

14   Southern Ocean. The surface salinity biases were again predominantly zonal, being up

15   to 0.2 psu too salty close to the Equator and in subpolar regions and the Arctic, and

16   too fresh in the subtropics. In the Labrador Sea and in the North Atlantic subpolar

17   gyre the surface waters are between 2° and 4°C too warm, and around 1 psu too salty.

18

19   Both GO1 and GO5.0 model configurations showed good skill in simulating oceanic

20   exchanges between North Atlantic, North Pacific and Arctic Oceans. The net oceanic

21   exports from the Arctic Ocean and the contributions from the individual straits are

22   within the uncertainties of the observational estimates. The main model bias is a more

23   vigorous exchange between the Atlantic and Arctic Oceans manifesting itself in too

24   strong (compared to observations) a northward flow of the buoyant warm Atlantic

25   water and too strong a return flow of the dense Arctic water as the overflows across

26   the Greenland-Scotland Ridge. The overturning circulation at 26°N in the Atlantic

27   was correspondingly stronger than that observed, at 21 Sv, The transport in the

28   Antarctic Circumpolar Current was 124 Sv, close to observed estimates, while the

29   Indonesian Throughflow was significantly higher than observations, most likely

30   because of insufficient mixing at the critical straits.

31

32   Comparison of the sea ice in the Northern Hemisphere in GO5.0 and observations

33   show that the model simulates the annual means, the interannual trend and the

1   seasonal cycle well, although the model underestimates summer sea ice extent. In the

2   Southern Hemisphere the sea ice extent again compares well with observations,

3   although the recent rising trend in sea ice cover is not simulated in GO5.0, as is also

4   the case in several other comparable models. Both GO1 and GO5.0 underestimate sea

5   ice volume in the Northern Hemisphere with biases larger in summer than in winter.

6   In the Southern Hemisphere the seasonal cycle of sea ice thickness is simulated

7   correctly, with a moderate underestimation (of 22% for GO5.0) of the hemisphere-

8   averaged sea ice thickness.

9

10 The main differences between GO5.0 and GO1 were seen in the penetration of heat

11 and salt into the interior ocean above the thermocline and in the representation of the

12 seasonal cycle. The global mean warming, with a maximum at 200 metres depth, was

13 reduced from 0.7° to 0.3°C, while the steady freshening trend at the same depth was

14 also reduced by 10-20%. Although the overall reduction in mixed layer depth from

15 GO1 to GO5.0 did not lead to unequivocal improvements in surface biases,

16 wintertime mixed layers were consistently better represented in GO5.0, while the

17 shallow bias in MLD and consequent warm surface bias in GO1 in tropical latitudes

18 were significantly ameliorated in GO5.0.

19

20 To attribute the changes seen between GO1 and GO5.0, the physics modifications

21 were applied incrementally (in most cases individually but some in pairs) starting

22 from the original GO1 configuration. First of all the NEMO source code was

23 upgraded from v3.2 to v3.4; then the model bathymetry was upgraded; the

24 background vertical diffusivity and viscosity were increased; some of the TKE

25 scheme parameters were adjusted; geothermal heat flux and double diffusion of

26 tracers were added; a scheme was added to represent a bottom boundary layer; and

27 finally modifications were made to the ice model. It was found that several of the

28 modifications led to changes with large spatial scales in the model surface and

29 subsurface fields that were distinguishable from the eddy variability, but the dominant

30 effects were traced to the code upgrade and to the TKE changes. These two changes,

31 which both affect mainly vertical mixing in the upper few hundred metres, were found

32 to produce most of the reduction of the subsurface temperature and salinity biases of

33 the model, along with the reduced errors in the seasonal cycle.

1

2 We conclude that GO5.0 represents a significant improvement in realism over the

3 previous configuration of the Met Office ocean model, GO1. In particular, the

4 improvements in the representation of vertical mixing (associated both with the code

5 upgrade from the NEMO v3.2 and in the modifications to the TKE vertical mixing

6 scheme in v3.4) lead to a more faithful simulation of the annual cycle in surface

7 temperature and mixed layer depth, as well as to reduced subsurface drifts in the

8 depth range 200-400 metres.

9

10 There are clearly aspects of the GO5.0 configuration that need to be improved further.

11 In particular, the subpolar North Atlantic and the Southern Ocean show substantial

12 errors in both surface and subsurface fields that may be at least partly ascribed to

13 deficiencies in model physics. Process Evaluation Groups (PEGs) have been set up

14 within the JOMP programme specifically to address issues relating to the two

15 aforementioned regions, and work is ongoing in both cases.

16

17 In addition, GO5.0 does not contain several physics upgrades which are currently

18 either available or under development in NEMO, and which offer potentially

19 significant improvements in model realism. These include embedded sea ice (in which

20 the base of the sea ice lies beneath the ocean surface and the ice displaces a non-zero

21 volume of sea water); and the z-tilde modification to the vertical coordinate to reduce

22 numerical mixing from high-frequency vertical motions (Leclair and Madec, 2011).

23 The full nonlinear free surface physics is available in NEMO v3.4, but not

24 implemented in GO5.0; it is expected that this, along with z-tilde and the embedded

25 ice, will be included in future implementations of the Global Ocean Model.

26

27

28 **Appendix A**

29

30 **Code availability and model trunk and branches**

31

32 The model code for NEMO v3.4 is available from the NEMO website (www.nemo-

33 ocean.eu). On registering, individuals can access the FORTRAN code using the open

source subversion software (http://subversion.apache.org/). The revision number of the base NEMO code (trunk) used for this paper is 3424. In addition we apply some modifications to the base code (branches). Please contact the authors for more information on these branches and how to obtain them.

The model code for CICE is freely available from the United States Los Alamos National Laboratory (http://oceans11.lanl.gov/trac/CICE/wiki/SourceCode), again using subversion. The revision number for the version used for this paper is 430 (trunk). Once again there are some additional modifications (branches) made for the purposes of this paper, and interested readers are requested to contact the authors for details.

UK users with access to PUMA (cms.ncas.ac.uk/wiki/PumaService) can copy the job details (job id xhimo) and submit a duplicate job using the Met Office Unified Model User Interface (UMUI).

Appendix B

FPP keys used in GO5.0 (NEMO and CICE)

key_dynspg_flt   Filtered free surface
key_ldfslp   Rotate diffusion operators (for tracer isopycnal diffusion)
key_traldf_c2d   Geographically varying lateral tracer diffusion
key_dynldf_c2d   Geographically varying lateral momentum diffusion
key_zdftke   TKE scheme for vertical mixing
key_zdftmx   Include tidal mixing scheme
key_zdfddm   Include double diffusive mixing parameterisation
key_trabbl   Include bottom boundary layer scheme

Appendix C

1   **Ocean and ice namelists for GO5.0**

2

3   These are included as supplementary material.

4

5

6   **Appendix D**

7

8   **Surface Forcing**

9

10   These are the CORE-2 forcing dataset (Large and Yeager 2008), available at

11   http://rda.ucar.edu/datasets/ds260.2/.

12

13

14   **Appendix E**

15

16   **Other input files.**

17

18   Other files such as bathymetry, river runoff mask and interpolation weights for the

19   surface forcing are required to run GO5.0. These can be obtained on request from the

20   authors.

21

1 **References**

2

3 Aagaard, K., T. Weingartner, S. L. Danielson, R. A. Woodgate, G. C. Johnson, and T.

4 E. Whitledge (2006), Some controls on flow and salinity in Bering Strait, Geophys.

5 Res. Lett., 33, L19602, doi:10.1029/2006GL026612.

6 Aksenov, Y., S. Bacon, A. Coward and N.P. Holliday, 2010. Polar Outflow from the

7 Arctic Ocean: A high resolution model study, J. Mar. Syst., 83(1-2), 14-37.

8 Amante, C. and B. W. Eakins, ETOPO1 1 Arc-Minute Global Relief Model:

9 Procedures, Data Sources and Analysis. NOAA Technical Memorandum NESDIS

10 NGDC-24, 19 pp, March 2009.

11 Arakawa, A. (1966), Computational design of long-term numerical integration of the

12 equations of fluid motion, J. Comput. Phys., 1, 119–143.

13 Arribas, A., M. Glover, A. Maidens, K. Peterson, M. Gordon, C. MacLachlan, R.

14 Graham, D. Fereday, J. Camp, A. A. Scaife, P. Xavier, P. McLean, A. Colman, S.

15 Cusack, 2011. The GloSea4 ensemble prediction system for seasonal forecasting Mon

16 Weather Rev 139 1891–1910 doi:10.1175/ 2010MWR3615.1.

17 Årthun, M., Nicholls, K. W., & Boehme, L. (2013). Wintertime Water Mass

18 Modification near an Antarctic Ice Front. Journal of Physical Oceanography, 43(2).

19 Axell, L. B., 2002: Wind-driven Internal Waves and Langmuir Circulations in a

20 Numerical Ocean Model of the Southern Baltic Sea. J. Geophys. Res., 107, 3204,

21 doi:10.1029/2001JC000922.

22

23 Barnier B., G. Madec, T. Penduff, J-M. Molines, A.-M. Treguier, J. Le Sommer, A.

24 Beckmann, A. Biastoch, C. Böning, J. Dengg, C. Derval, E. Durand, S. Gulev, E.

25 Remy, C. Talandier, S. Theetten, M. Maltrud, J. McClean, and B. De Cuevas, 2006.

26 Impact of partial steps and momentum advection schemes in a global ocean

27 circulation model at eddy permitting resolution. Ocean Dynamics, Vol 4, DOI

28 10.1007/s10236-006-0082-1.

29 Beckmann, A., and R. Doescher, 1997, A Method for Improved Representation of

Dense Water Spreading over Topography in Geopotential-Coordinate Models, J. Phys. Oceanogr., 27, 581-591

Bitz, C.M., Lipscomb, W.H., 1999. An energy-conserving thermodynamic model of sea ice. Journal of Geophysical Research 104, 15669-15677.

Bitz, C. M., Holland, M., Eby, M., Weaver, A.J., 2001. Simulating the ice-thickness distribution in a coupled climate model. Journal of Geophysical Research 106, 2441–2463.

Blaker, A.T., J.J-M. Hirschi, G. McCarthy, B. Sinha, S. Taws, R. Marsh, A.C. Coward and B.A. de Cuevas, 2013. Historical analogues of the recent extreme minima observed in the Atlantic meridional overturning circulation at 26°N. Climate Dynamics, in press.

Blanke, B. and P. Delecluse, 1993. Variability of the tropical Atlantic ocean simulated by a general circulation model with two different mixed layer physics. J. Phys. Oceanogr., 23, 1363-1388.

Bourdalle-Badie, R. & Treguier, A.-M., 2006, A climatology of runoff for the global ocean-ice model ORCA025, Report, Mercator-Ocean, MOO-RP-425-365-MER

de Boyer Montégut, C., G. Madec, A. S. Fischer, A. Lazar, and D. Iudicone (2004), Mixed layer depth over the global ocean: an examination of profile data and a profile-based climatology, J. Geophys. Res., 109, C12003

Brown, A., S. Milton, M. Cullen, B. Golding, J. Mitchell and A. Shelley, 2012, Unified Modeling and Prediction of Weather and Climate: A 25-Year Journey. Bull. Amer. Meteor. Soc. 93 1865–1877

Calvert, D., and J. Siddorn, 2013. Revised vertical mixing parameters for the UK community standard configuration of the global NEMO ocean model, Hadley Centre Technical Note, 95.

Cavalieri, D. J., C. L. Parkinson, P. Gloersen, and H. Zwally. 1996, updated yearly. Sea Ice Concentrations from Nimbus-7 SMMR and DMSP SSM/I-SSMIS Passive

Microwave Data. [indicate subset used]. Boulder, Colorado USA: NASA DAAC at the National Snow and Ice Data Center.

Clement Kinney, J., W. Maslowski, Y. Aksenov, B. de Cuevas, A. Nguyen, R. Osinski, M. Steele, R.A. Woodgate and J. Zhang, 2014. On the Flow Through Bering Strait: A Synthesis of Model Results and Observations, in "The Pacific Arctic Region. Ecosystem Status and Trends in a Rapidly Changing Environment". Grebmeier, Jacqueline M., Maslowski, Wieslaw (Eds.).

Collins, W.J., N. Bellouin, M. Doutriaux-Boucher, N. Gedney, T. Hinton, C. D. Jones, S. Liddicoat, G. Martin, F. O'Connor, J. Rae, C. Senior, I. Totterdell, S. Woodward, T. Reichler, J. Kim, 2008: Evaluation of the HadGEM2 model. Met Office Hadley Centre Technical Note no. HCTN 74, available from Met Office, FitzRoy Road, Exeter EX1 3PB http://www.metoffice.gov.uk/publications/HCTN/index.html

Craig, P. D., and M. L. Banner, 1994: Modelling Wave-Enhanced Turbulence in the Ocean Surface Layer. J. Phys. Oceanogr., 24, 2546-2559.

Culverwell, I. (2009), private communication

Cunningham, S.A., S. G. Alderson, B. A. King, and M. A. Brandon, 2003: Transport and variability of theAntarctic Circumpolar Current in Drake Passage. J. Geophys. Res., 108C, 8084, doi:10.1029/2001JC001147.

Cuny, J., P. Rhines, and R. Kwok, R. (2005), Davis Strait volume, freshwater and heat fluxes. Deep-Sea Res. I, 52, 519-542.

Curry, B., C. M., Lee, and B. Petrie (2010), Volume, freshwater, and heat fluxes through Davis Strait, 2004-05, J. Phys. Oceanogr., 10.1175/2010JPO4536.1.

Dai, A., and K. E. Trenberth (2002), Estimates of freshwater discharge from continents: latitudinal and seasonal variations, J. Hydrometeorol., 3, 660-687.

Danabasoglu, G. W. Large & B. Briegleb (2010) Climate impacts of parameterized Nordic Sea overflows. J. Geophys. Res., 115, C11005

Dawson, A.; A.J. Matthews, D.P. Stevens, M.J. Roberts & P-L. Vidale, (2012) Importance of oceanic resolution and mean state on the extra-tropical response to El Nino in a matrix of coupled models. Clim. Dyn., Online First. doi:10.1007/s00382-012-1518-6

Delworth, T., A. Rosati, W. Anderson, A. Adcroft, V. Balaji, R. Benson, K. Dixon, S. Griffies, H. Lee, R. Pacanowski & others (2012) Simulated climate and climate change in the GFDL CM2. 5 high-resolution coupled climate model. J. Climate, 25, 2755-2781

Farneti, R., T. L. Delworth, A. J. Rosati, S. M. Griffies, and F. Zeng (2010), The role of mesoscale eddies in the rectification of the Southern Ocean response to climate change. J. Phys. Oceanogr., 40, 1539{1557, doi:10.1175/2010JPO4353.1.

Farneti, R. and P.R. Gent, 2011: The effects of the eddy-induced advection coefficient in a coarse-resolution coupled climate model, Ocean Modelling, 39, Issues 1–2, 135-145, doi: http://dx.doi.org/10.1016/j.ocemod.2011.02.005.

Gammelsrod, T., O. Leikvin, V. Lien, W. P. Budgell, H. Loeng, and W. Maslowski (2009), Mass and heat transports in the NE Barents Sea: Observations and models, Journal of Marine Systems, 75(1-2), 56-69, doi:10.1016/j.jmarsys.2008.07.010.

Gaspar, P., Y. Grégoris, and J. –M. Lefevre, 1990: A simple eddy kinetic energy model for simulations of the oceanic vertical mixing: Tests at Station Papa and long-term upper ocean study site. J. Geophys. Res., 95(C9), 16179-16193, doi:10.1029/JC095iC09p16179.

Gent, P.R. and G. Danabasoglu, 2011: Response to Increasing Southern Hemisphere Winds in CCSM4. J. Climate, 24, 4992–4998. doi: http://dx.doi.org/10.1175/JCLI-D-10-05011.1

Gent, P.R. and J.C. McWilliams, (1990), "Isopycnal mixing in ocean circulation

1   models", J. Phys. Ocean. 20 pp. 150-155

2

3   Gnanadesikan, A., S.M. Griffies & B.L. Samuels (2007): Effects in a climate model

4   of slope tapering in neutral physics schemes. Ocean Modelling 16 (1), 1-16.

5

6   Gordon, C., C. Cooper, C. A. Senior, H. Banks, J. M. Gregory, T. C. Johns, J. F. B.

7   Mitchell, and R. A. Wood, 2000: The simulation of SST, sea ice extents and ocean

8   heat transports in a version of the Hadley Centre coupled model without flux

9   adjustments. Clim. Dyn., 16, 147–168.

10 Gregg, M.C, T.B. Sanford & D.P. Winkel, 2003. Reduced mixing from the breaking

11 of internal waves in equatorial waters. Nature 422, 513-515

12 Greatbatch, R. J., and K. A. Peterson (1996), Interdecadal variability and oceanic

13 thermohaline   adjustment,   J.   Geophys.   Res.,   101(C9),   20467–20482,

14 doi:10.1029/96JC01531.

15

16 Griffies, S.M., R.C. Pacanowski and R.W. Hallberg, 2000. Spurious diapycnal mixing

17 associated with advection in a z-coordinate ocean model. Monthly Weather Review

18 128 (3), 538-564.

19

20 Griffies, S.M., A. Biastoch, C. Böning, F. Bryan, G. Danabasoglu, E.P. Chassignet,

21 M.H. England, R. Gerdes, H. Haak, R.W. Hallberg, W. Hazeleger, J. Jungclaus, W.

22 G. Large, G. Madec, A. Pirani, B.L. Samuels, M. Scheinert, A. Sen Gupta, C.A.

23 Severijns, H.L. Simmons, A-M Treguier, M. Winton, S. Yeager, J. Yin, 2008.

24 Coordinated Ocean-ice Reference Experiments (COREs), Ocean Modelling 26, Issues

25 1–2, 1-46. doi:10.1016/j.ocemod.2008.08.007.

26

27 Hallberg, R., and A. Gnanadesikan (2006), The role of eddies in determining the

28 structure and response of the wind-driven southern hemisphere overturning: Results

29 from the Modeling Eddies in the Southern Ocean (MESO) project., J. Phys.

30 Oceanogr., 36, 2232-2252.

31

Hewitt, H.T., D. Copsey, I. D. Culverwell, C. M. Harris, R. S. R. Hill, A. B. Keen, A. J. McLaren and E. C. Hunke, 2011. Design and implementation of the infrastructure of HadGEM3: the next-generation Met Office climate modelling system. Geosci. Model Dev., 4, 223–253, doi:10.5194/gmd-4-223-2011.

Hirschi, J.J.-M.. A. T. Blaker, B. Sinha, A. Coward, B. de Cuevas, S. Alderson, and G. Madec, 2013. Chaotic variability of the meridional overturning circulation on subannual to interannual timescales. Ocean Sci., 9, 805–823, doi:10.5194/os-9-805-2013

Holland, P. R., and R. Kwok (2012), Wind-driven trends in Antarctic sea-ice drift, Nature Geosci, 5, 872–875, doi:10.1038/ngeo1627.

Houghton, J. T., Y. Ding, D. J. Griggs, M. Noguer, P. J. van der Linden, and D. Xiaosu, Eds., 2001: Climate Change 2001: The Scientific Basis. Cambridge University Press, 944 pp.

Hunke, E.C. and J.K. Dukowicz, 1997. An Elastic–Viscous–Plastic Model for Sea Ice Dynamics. J. Phys. Oceanogr., 27, 1849-1867.

Hunke, E.C., Lipscomb, W.H., 2010. CICE: The Los Alamos Sea Ice Model, Documentation and Software User's Manual, Version 4.1. Tech. Rep. LA-CC- 06-012, Los Alamos National Laboratory, Los Alamos, New Mexico. http://oceans11.lanl.gov/trac/CICE.

Ingleby, B and M. Huddleston, 2007. Quality control of ocean temperature and salinity profiles - historical and real-time data. J. Mar. Sys., 65,158-175.

IOC, IHO and BODC, 2003. Centenary Edition of the GEBCO Digital Atlas, published on CD-ROM on behalf of the Intergovernmental Oceanographic Commission and the International Hydrographic Organization as part of the General Bathymetric Chart of the Oceans, British Oceanographic Data Centre, Liverpool, U.K.

1

2 Johns, T. C., and Co-authors, 2006: The New Hadley Centre Climate Model

3 (HadGEM1): Evaluation of coupled simulations. J. Climate, 19, 1327–1353.

4

5 Josey, S. A., S. Gulev and L. Yu, 2013: Exchanges through the ocean surface, in

6 Siedler, G., Griffies, S., Gould, J. and Church, J. (Eds.): Ocean Circulation and

7 Climate 2nd Ed. A 21st century perspective, Academic Press, International

8 Geophysics Series, Volume 103, p. 115-140.

9

10 Kennedy J.J., Rayner, N.A., Smith, R.O., Saunby, M. and Parker, D.E., 2011:

11 Reassessing biases and other uncertainties in sea-surface temperature observations

12 measured in situ since 1850 part 2: biases and homogenisation. Journal of

13 Geophysical Research, 116, doi:10.1029/2010JD015220

14

15 Koch-Larrouy A., G. Madec, B. Blanke and R. Molcard, 2008: Water mass

16 transformation along the Indonesian throughflow in an OGCM. Ocean Dynamics, 58,

17 289-309.

18

19 Large, W.G. and S.G. Yeager, 2008. The Global Climatology of an Interannually

20 Varying Air-Sea Flux Data Set. Climate Dynamics, doi:10.1007/s00382-008-0441-3.

21

22 Leclair and G. Madec (2011), Ocean Modelling 37 pp 139-152

23 Lee, M-M, A.C. Coward and A.J.G. Nurser, 2002. Spurious diapycnal mixing of the

24 deep waters in an eddy-permitting global ocean model. J. Phys. Oceanog. 32, 1522-

25 1535.

26 Lohmann, G., Gerdes, R., and Chen, D., 1996. Sensitivity of the thermohaline

27 circulation in coupled oceanic GCM-atmospheric EBM experiments. Climate

28 Dynamics 12, 403-416.

29

Madec, G.. 2008. NEMO - the OPA9 ocean engine. Note du Pole de Modelisation. Institut Pierre-Simion Laplace. 1:100 pp. http://www.nemo-ocean.eu/content/download/21612/97924/file/NEMO_book_3_4.pdf

McCarthy, G., E. Frajka-Williams, W.E. Johns, M.O. Baringer, C.S. Meinen, H.L. Bryden, D. Rayner, A. Duchez, C. Roberts, and S.A. Cunningham, 2012. Observed interannual variability of the Atlantic meridional overturning circulation at 26.5°N. Geophys. Res. Lett 39, L19609, doi:10.1029/2012GL052933

Megann, A. P., A. L. New, A. T. Blaker, and B. Sinha, 2010. The sensitivity of a coupled climate model to its ocean component. J. Climate, 23, 5126–5150.

Meijers, A. J. S., E. Shuckburgh, N. Bruneau, J.-B. Sallee, T. J. Bracegirdle, and Z. Wang (2012) Representation of the Antarctic Circumpolar Current in the CMIP5 climate models and future changes under warming scenarios. J. Geophys. Res., 117, C12008, doi:10.1029/2012JC008412.

Meredith, M. P., et al. (2011), Sustained monitoring of the Southern Ocean at Drake Passage: Past achievements and future priorities, Rev. Geophys., 49, RG4005, doi:10.1029/2010RG000348.

Merryfield, W.J., G. Holloway and A.E. Gargett, 1999, A Global Ocean Model with Double-Diffusive Mixing, J. Phys. Ocean. 29,1124-1142

Munday, D.R., H.L. Johnson, D.P. Marshall, 2013: Eddy Saturation of Equilibrated Circumpolar Currents. J. Phys. Ocean. 43, 507–532. doi: http://dx.doi.org/10.1175/JPO-D-12-095.1

Olsen, Steffen M., et al. "Observed and modelled stability of overflow across the Greenland–Scotland ridge." Nature 455.7212 (2008): 519-522.

Østerhus, S., Turrrell,W.R., Jónsson, S., Hansen, B., 2005. Measured volume, heat, and salt fluxes from the Atlantic to the Arctic Mediterranean. Geophys. Res. Lett. 32, L07603.

Penduff, T., J. Le Sommer, B. Barnier, A.-M. Treguier, J.-M.Molines, G. Madec, 2007. Influence of numerical schemes on current-topography interactions in 1/4° global ocean simulations. Ocean Sci. 3, 509-524.

Penduff, T., M. Juza, L. Brodeau, G. Smith, B. Barnier, J. Molines, A. Treguier, & G. Madec (2010): Impact of global ocean model resolution on sea-level variability with emphasis on interannual time scales Ocean Sci., 6, 269-284

Rae, J.G.L., Hewitt, H.T., Keen, A.B., Ridley, J.K., Harris, C.M., Hunke, E.C. and Walters, D.N. (2013). Development of Global Sea Ice 5.0 CICE configuration. J. Geoscientific Model Dev. In preparation.

Rahmstorf, Stefan, Jürgen Willebrand, 1995: The Role of Temperature Feedback in Stabilizing the Thermohaline Circulation. J. Phys. Oceanogr., 25, 787–805. doi: 10.1175/1520-0485

Rayner, N. A.; Parker, D. E.; Horton, E. B.; Folland, C. K.; Alexander, L. V.; Rowell, D. P.; Kent, E. C.; Kaplan, A. (2003) Global analyses of sea surface temperature, sea ice, and night marine air temperature since the late nineteenth century J. Geophys. Res.108, No. D14, 4407 10.1029/2002JD002670).

Remy E., L. Siefridt, L. Fleury and M. Bremond, 2003: Construction de la bathymetrie pour la configuration modele ORCA025, CERFACS Report, May 2003.

Reynolds, R.W., N.A. Rayner, T.M., Smith, D.C. Stokes, and W. Wang, 2002: An Improved In Situ and Satellite SST Analysis for Climate, J. Climate 15, 1609-1625.

Roberts, C.D., J. Waters, K.A. Peterson, M.D. Palmer, G.D. McCarthy, E. Frajka-Williams, K. Haines, D.J. Lea, M.J. Martin, D. Storkey, E.W. Blockley, H. Zuo, 2013.

Atmosphere drives recent interannual variability of the Atlantic meridional overturning circulation at 26.5°N. Geophysical Research Letters, 40 (19). 5164-5170. 10.1002/grl.50930

Roberts, M J., A. Clayton, M-E. Demory, J. Donners, P-L. Vidale, W. Norton, L. Shaffrey, D.P. Stevens, I. Stevens, R.A. Wood, J. Slingo, 2009. Impact of Resolution on the Tropical Pacific Circulation in a Matrix of Coupled Models. J. Climate, 22, 2541–2556.

Robson, J, D. Hodson, E. Hawkins and R. Sutton, 2014. Atlantic overturning in decline? Nature Geoscience 7, 2-3

Saunders, P.P., S.A Cunningham, B.A.de Cuevas and A.C. Coward, 2008. Comments on "Decadal Changes in the North Atlantic and Pacific Meridional Overturning Circulation and Heat Flux". J. Phys. Ocean. 38, 2104-2107.

Scaife, A.A., D. Copsey, C. Gordon, C. Harris, T. Hinton, S. Keeley, A. O'Neill, M. Roberts, K. Williams, 2011. Improved Atlantic winter blocking in a climate model. Geophys. Res. Lett. 38 issue 23, L23703

Semtner, A.J. (1976), A model for the thermodynamic growth of sea ice in numerical investigations of climate, J. Phys. Oceanogr., 6, 379-389.

Shaffrey, L.C., I. Stevens, W.A. Norton, M.J. Roberts, P.L. Vidale, J. D. Harle, A. Jarrar, D.P. Stevens, M.J. Woodage, M.E. Demory, J. Donners, D.B. Clark, A. Clayton, J.W. Cole, S.S. Wilson, W.M. Connolley, T.M. Davies, A.M. Iwi, T.C. Johns, J.C. King, A.L. New, J.M. Slingo, A. Slingo, L. Steenman-Clark, and G.M. Martin, 2009. U.K. HiGEM: The New U.K. High-Resolution Global Environment Model—Model Description and Basic Evaluation. J. Climate 22 (8), 1861–1896

Simmons, H., Jayne, S., Laurent, L.S. & Weaver, A., 2004, Tidally driven mixing in a numerical model of the ocean general circulation, Ocean Modelling 6 245-263

Sinha, B, B. Topliss, A. T. Blaker and J. J.-M. Hirschi (2013) A numerical model study of the effects of interannual timescale wave propagation on the predictability of the Atlantic meridional overturning circulation, J. Geophys. Res., 118, 131-146, doi:10.1029/2012JC008334.

Skagseth, Ø., Furevik, T., Ingvaldsen, R., Loeng, H., Mork, K.A., Orvik, K.A., Ozhigin, V., 2008. Volume and heat transports to the Arctic Ocean via the Norwegian and Barents Seas. In: Dickson, R.R., Meincke, J., Rhines, P. (Eds.), Arctic–Subarctic Ocean Fluxes: Defining the Role of the Northern Seas in Climate. Springer Verlag, Netherlands, pp. 45–64.

Sirevaag, A., M.G. McPhee, J.H. Morison, W.J. Shaw, and T.P. Stanton, 2010. Wintertime mixed layer measurements at Maud Rise, Weddell Sea. J. Geophys. Res., 115, C02009, doi:10.1029/2008JC005141.

Smeed, D.A., G. McCarthy, S.A. Cunningham, E. Frajka-Williams, D. Rayner, W.E. Johns, C.S. Meinen, M.O. Baringer, B.I. Moat, A. Duchez and H.L. Bryden, 2013. Ocean Sci. Discuss., 10, 1619–1645, 2013. www.ocean-sci-discuss.net/10/1619/2013/, doi:10.5194/osd-10-1619-2013

Smith DM Cusack S Colman AW Folland CK Harris GR Murphy JM (2007) Improved surface temperature prediction for the coming decade from a global climate model. Science 317 796-799 doi:10.1126/science.1139540.

Solomon, S., D. Qin, M. Manning, Z.Chen, M. Marquis, K. B. Averyt, M. Tignor, and H. L. Miller, Eds., 2007: Climate Change 2007: The Physical Science Basis. Cambridge University Press, 996 pp.

Sprintall, J., S. E. Wijffels, R. Molcard, and I. Jaya (2009), Direct estimates of the Indonesian Throughflow entering the Indian Ocean: 2004–2006, J. Geophys. Res., 114, C07001, doi:10.1029/2008JC005257.

1   Stein, C. A. and S. Stein, 1992 : A model for the global variation in oceanic depth and

2   heat flow with lithospheric age. Nature, 359, 123–129.

3

4   Storkey, D., E.W. Blockley, R. Furner, C. Guiavarc'h, D. Lea, M.J. Martin, R.M.

5   Barciela, A. Hines, P. Hyder, J.R. Siddorn, 2010. Forecasting the ocean state using

6   NEMO: The new FOAM system. Journal of Operational Oceanography, Volume

7   3, Number 1, pp. 3-15

8

9   Tansley, C. E., and D. P. Marshall (2001a), On the dynamics of wind-driven

10   circumpolar currents., J. Phys. Oceanogr., 31, 3258-3273.

11

12   Thomas, M. D. and X. Zhai, 2013. Eddy-induced variability of the meridional

13   overturning circulation in a model of the North Atlantic. Geophys. Res. Lett,. 40, 1–6,

14   doi: 10.1002/grl.50532, 2013

15

16   Viebahn, J., and C. Eden (2010), Towards the impact of eddies on the response of the

17   Southern Ocean to climate change. Ocean Modell., 34, 150-165.

18

19   Williamson, D., M. Goldstein, L. Allison, A. Blaker, P. Challenor, L. Jackson.,

20   2013. History matching for the quantification and reduction of parametric uncertainty

21   in climate model projections. Climate Dynamics, in press.

22

23   Woodgate, R. A., T. J. Weingartner, and R. Lindsay (2012), Observed increases in

24   Bering Strait oceanic fluxes from the Pacific to the Arctic from 2001 to 2011 and their

25   impacts on the Arctic Ocean water column, Geophys. Res. Lett., 39, L24603,

26   doi:10.1029/2012GL054092.

27

28   Worby, A. P., C. Geiger, M. J. Paget, M. van Woert, S. F Ackley, T. DeLiberty,

29   (2008). Thickness distribution of Antarctic sea ice. J. Geophys. Res., 113, C05S92,

30   doi:10.1029/2007JC004254.

31

32   Yeager, S. G. and M. Jochum, 2009. The connection between Labrador Sea buoyancy

33   loss, deep western boundary current strength, and Gulf Stream path in an ocean

1 circulation model. Ocean Modelling 30, Issues 2–3, 207-224.

2

3 Zalesak, S. T., 1979, Fully multidimensional flux corrected transport algorithms for

4 fluids. J. Comput. Phys. 31.

5

6 Zhang, J., D.R. Thomas, D.A. Rothrock, R.W. Lindsay, Y. Yu, and R. Kwok,

7 "Assimilation of ice motion observations and comparisons with submarine ice

8 thickness data", J. Geophys. Res., 108, 10.1029/2001JC001041, 2003.

9

1   **Figure captions**

2

3   <u>Figure 1</u> Surface biases in years 1996-2005 of GO5.0: (a) mean surface temperature

4   bias with respect to the Reynolds et al climatology; and (b) mean surface salinity bias

5   with respect to the EN3 climatology.

6

7   <u>Figure 2</u> Seasonal cycle of mixed-layer depth (MLD) in GO5.0: (a) minimum

8   monthly MLD in years 1996-2005; (b) minimum monthly MLD in the deBoyer

9   Montegut et al. climatology; (c) maximum monthly MLD in years 1996-2005; and (d)

10   maximum monthly MLD in the deBoyer Montégut et al climatology. The hatching in

11   panels a and b correspond to the areas of missing ocean data in panels c and d, where

12   a full annual cycle of MLD is not observed in the de Boyer Montégut climatology.

13

14   <u>Figure 3</u> Zonal mean (a) temperature and (b) salinity biases in years 1996-2005 of

15   GO5.0. The solid contours are of the zonal mean potential density σ_0, with a spacing

16   of 0.5 kg m^3.

17

18   <u>Figure 4</u> (a) Time series of annual mean Atlantic meridional overturning circulation

19   (AMOC) at 26°N in GO1 and GO5.0, with the potential density σ_0 in the upper 200

20   metres in the central Labrador Sea; and (b) mean Atlantic overturning streamfunction

21   in years 1996-2005 of GO1 (left) and GO5.0 (right). Note that velocity data are

22   missing in years 1986-1990 of GO1 .

23

24   <u>Figure 5</u> Time series of integrated sea ice properties in GO5.0 (red) and from

25   observational estimates (blue): (a) Arctic mean ice extent; (b) Arctic mean ice

26   volume; (c) Antarctic mean ice extent; and (d) Antarctic mean ice volume.

27

28   <u>Figure 6</u> High-latitude sea ice extent in GO5.0 and in the HadISST observational

29   dataset: Arctic winter (DJF) ice extent in (a) GO5.0 and (b) observations; Antarctic

30   winter (JJA) ice extent in (c) GO5.0 and (d) observations; Arctic summer (JJA) ice

31   extent in (e) GO5.0 and (f) observations; and Antarctic summer (DJF) ice extent in (g)

32   GO5.0 and (h) observations.

33

1   Figure 7 Subsurface drifts, defined as the difference of the horizontally-averaged

2   annual mean in any year from that in the first year of integration, as function of depth:

3   (a) GO1 temperature drift; (b) GO5.0 temperature drift; (c) GO1 salinity drift; and (d)

4   GO5.0 salinity drift.

5

6   Figure 8 Seasonal sea surface temperature (SST) biases against Reynolds et al

7   climatology: boreal winter (DJF) biases in (a) GO1 and (b) GO5.0; and boreal

8   summer (JJA) biases in (c) GO1 and (d) GO5.0.

9

10   Figure 9 Monthly sea surface temperature (SST) and mixed layer depth (MLD) biases

11   against Reynolds et al and de Boyer Montégut et al climatology, respectively, in years

12   1996-2005 as a function of latitude: (a) GO1 SST; (b) GO5.0 SST; (c) GO1 MLD;

13   and (d GO5.0 (monthly) MLD.

14

15   Figure 10. (a) Zonal mean net air–sea heat flux in GO1 (black); GO5.0 (red) and

16   CORE2 data (dashed blue line) in years 1996-2005; and (b) surface net downward

17   heat flux difference GO5.0 minus GO1. This figure is adapted from Fig 5.10 of Josey

18   et al, 2013

19

20   Figure 11 Effect on sea surface fields in years 1981-1985 of ocean code upgrade from

21   v3.2 (GO1) to v3.4 (N3.4): (a) GO1 SST bias; (b) N3.4 SST bias; (c) N3.4 minus

22   GO1 SST; (d) GO1 SSS bias; (e) N3.4 SSS bias; and (f) N3.4 minus GO1 SSS.

23

24   Figure 12 Effect on zonal mean temperature in years 1981-1985 of code upgrade from

25   NEMO v3.2 (GO1) and v3.4 (experiment N3.4) in years 1981-1985. (a) bias in GO1;

26   (b) bias in N3.4; and (c) difference N3.4 minus GO1. The solid contours are of the

27   zonal mean potential density σ_0 in N3.4, with a spacing of 0.5 kg m^3.

28

29   Figure 13 Effect on sea surface fields in years 1981-1985 of TKE scheme changes

30   (from experiment N3.4_vmix to N3.4_tke): (a) N3.4_vmix SST bias; (b) N3.4_tke

31   SST bias; (c) N3.4_tke minus N3.4_vmixSST; (d) N3.4_vmix SSS bias; (e) N3.4_tke

32   SSS bias; and (f) N3.4_tke minus N3.4_vmix SSS.

33

1   Figure 14 Effect on zonal mean temperature in years 1981-1985 of TKE scheme
2   changes (from experiment N3.4_vmix to N3.4_tke). (a) bias in N3.4_vmix; (b) bias in
3   N3.4_tke; and (c) difference N3.4_tke minus N3.4_vmix. The solid contours are of
4   the zonal mean potential density σ_0 in N3.4_tke, with a spacing of 0.5 kg m^3.
5

Parameter	GO1 (where different from GO5)	GO5
Horizontal bilapacian viscosity	Same as in GO5.0	$-1.5 \times 10^{11}\,\mathrm{m^4 s^{-1}}$
Isoneutral laplacian tracer diffusion	Same as in GO5.0	$300\,\mathrm{m^2 s^{-1}}$
Background vertical viscosity	$1.0 \times 10^{-4}\,\mathrm{m^2 s^{-1}}$	$1.2 \times 10^{-4}\,\mathrm{m^2 s^{-1}}$
Background vertical diffusivity	$1.0 \times 10^{-5}\,\mathrm{m^2 s^{-1}}$	$1.2 \times 10^{-5}\,\mathrm{m^2 s^{-1}}$
Energy coefficient for Craig and Banner (1994) surface wave breaking parameterisation	60.0	67.83
Length scale for near-inertial wave breaking parameterisation	0.5 m in tropics, rising to 30 m at midlatitudes	10 m everywhere
Minimum value of surface mixing length scale	0.01 m	0.04 m
Minimum value of interior mixing length scale	0.001 m	0.01 m

1

2   **Table 1.** Parameter changes between GO1 and GO5.0.

3

1

Run name	UM job id	NEMO vn.	rn_avt0 x10^{-5}	bathy	rn_mxl0	rn_ebb	nn_htau	nn_geoflx	Run (years)
GO1	xexoc	3.2	1.0	G70	n/a	60.0	1	0	30
N3.4	xhiml	3.4	1.0	G70	0.001	60.0	1	0	30
N3.4_mxl0	xhimq	3.4	1.0	G70	0.01	60.0	1	0	30
N3.4_bath	xhimj	3.4	1.0	GO5	0.001	60.0	1	0	10
N3.4_vmix	xhkfg	3.4	1.2	GO5	0.001	60.0	1	0	10
N3.4_tke	xhkfi	3.4	1.2	GO5	0.04	67.83	0	0	10
N3.4_geo	xhimt	3.4	1.2	GO5	0.04	67.83	0	2	10
N3.4_DD	xhimp	3.4	1.2	GO5	0.04	67.83	0	2	10
N3.4_ice	xhimm	3.4	1.2	GO5	0.04	67.83	0	2	10
N3.4_bbl	xhimn	3.4	1.2	GO5	0.04	67.83	0	2	10
GO5.0	xhimo	3.4	1.2	GO5	0.04	67.83	0	2	30

2

3　　**Table 2** Summary of integrations carried out. The UM job id is a unique identifier

4　　for each run within the Met Office Unified Model system, and allows any

5　　configuration to be replicated by another user. The parameters listed are: *rn_avt0*

6　　(background vertical tracer diffusivity)*; rn_mxl0 (*minimum surface mixing length

7　　scale); and *rn_ebb (*coefficient of the surface input of TKE). The switch *nn_htau*

8　　enables a spatially varying TKE penetration depth scale, while *nn_geoflx* applies

9　　an abyssal geothermal heat flux.

10

11

1

Location	Observed value	GO1	GO5.0
AMOC at 26°N	$18.5 \pm 1^{(1)}$	21.0 ± 4.2	22.0 ± 4.2
Barents Sea Opening net	$2.8 \pm 0.6^{(2,3,4)}$	3.3 ± 2.0	3.0 ± 2.0
Fram Strait net	$-2.3 \pm 4.3^{(5)}$	-1.9 ± 2.4	-1.6 ± 2.3
Denmark Strait net	$(-6.0 \text{ to } -3.6)^{(4)}$	-3.4 ± 3.3	-3.3 ± 3.3
Denmark Strait overflow$^{(*)}$	$-2.9 \pm 0.6^{(6)}$	-5.3 ± 2.9	-4.34 ± 2.1
Iceland-Faeroes net	$2.8 \pm 0.5^{(7)}$	2.72 ± 1.2	2.6 ± 1.2
Iceland-Faeroes overflow$^{(*)}$	$-1.0 \pm 0.5^{(6)}$	-0.9 ± 0.5	-0.9 ± 0.5
Faeroes-Scotland net	$1.8 \pm 0.5^{(7)}$	1.4 ± 2.3	1.7 ± 2.3
Faeroes-Scotland overflow$^{(*)}$	$-2.4 \pm 0.4^{(6)}$	-3.1 ± 0.8	-3.1 ± 0.9
Total Greenland-Scotland inflow$^{(**)}$	$8.5 \pm 1.0^{(7)}$	9.3 ± 1.8	10.0 ± 1.7
Bering Strait net	$0.8 [1.1^{(+)}] \pm 0.2^{(9)}$	1.3 ± 0.9	1.4 ± 0.9
Davis Strait net$^{(***)}$	-2.6 ± 1.0 to $-2.3 \pm 0.7^{(5,8)}$	-2.9 ± 1.2	-3.0 ± 1.1
Drake Passage	$135 \pm 20^{(10)}$	119 ± 8	124 ± 8
Indonesian Throughflow	$-15 \pm 4^{(11)}$	-19.7 ± 5.4	-19.8 ± 5.5

2

3 **Table 3** Volume transports (Sv), observed and model mean values and their standard

4 deviations. Model values are means over the last 10 years of the 30 years spin up.

5 Model standard deviations are obtained from the 5-day averages. Sign convention is

6 positive northwards and eastwards, and is negative southwards and westwards. Key:

7 [1] McCarthy et al 2012, [2]Gammelsrod et al., 2009, [3]Skagseth, et al., 2008, [4]Aksenov

8 et al., 2010, [5]Curry et al., 2011, [6]Olsen et al., 2008, [7]Østerhus et al., 2005, [8]Cuny et

9 al., 2005, [9]Woodgate et al., 2012, [10]Cunningham et al., 2003, [11]Sprintall et al., 2009,

10 [+]climatological transport with the estimate for 2011 in parenthesis, [*]southward

11 transport of waters with $\sigma_\theta > 27.8$, [**]Atlantic inflow derived as the residual flow after

12 subtracting the southward transport of waters with $\sigma_\theta > 27.8$, [***]including transports on

13 the West Greenland Shelf.

14
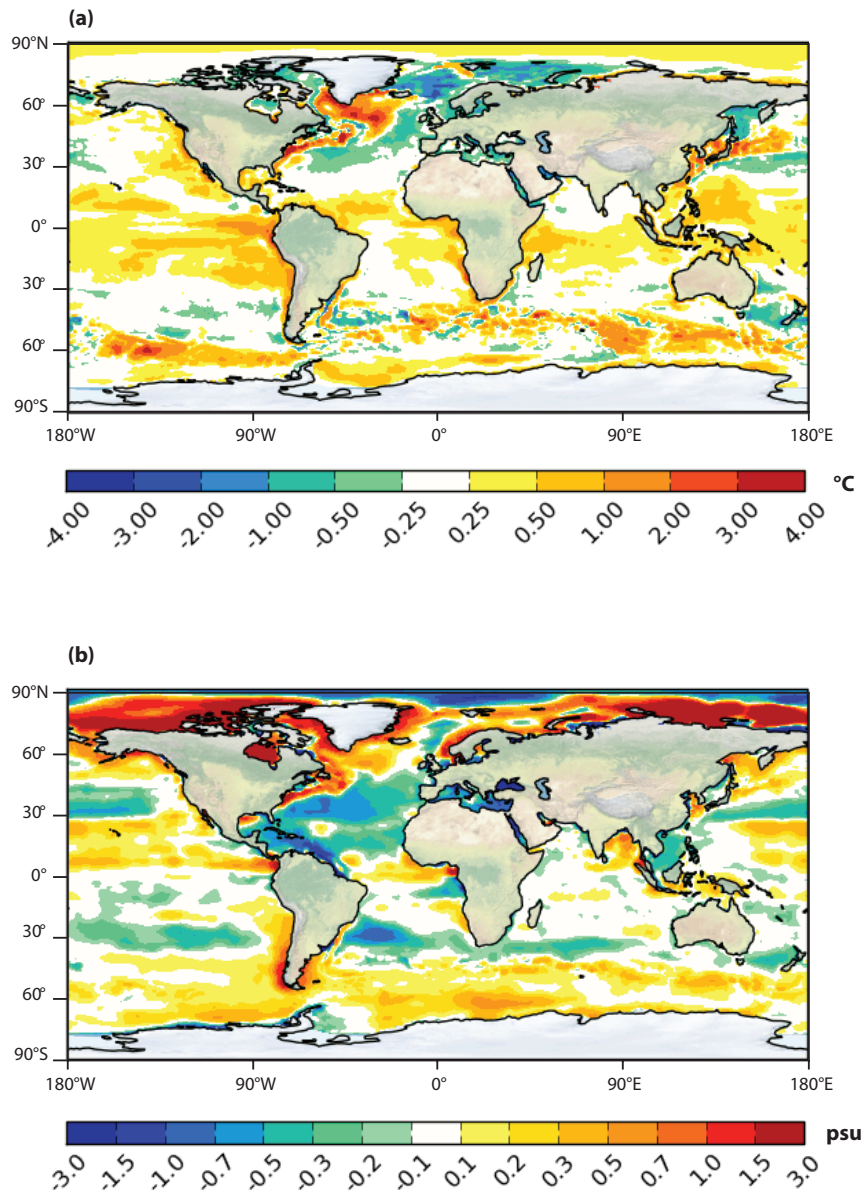
(a)

(b)

Figure 1. Surface biases in years 1996-2005 of GO5.0: (a) mean surface temperature bias with respect to the Pathfinder climatology; and (b) mean surface salinity bias with respect to the EN3 climatology.

1

1
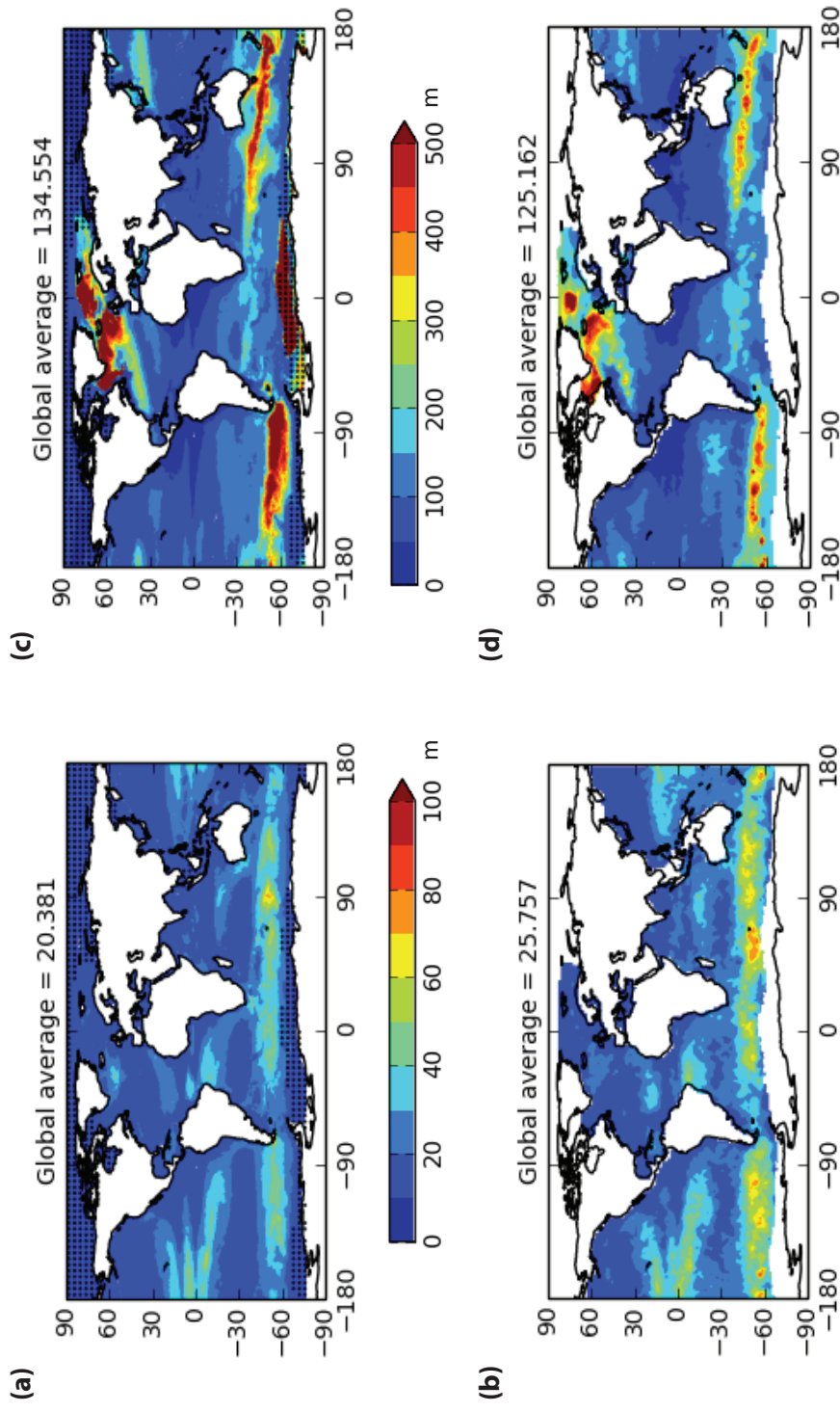
Figure 2 Seasonal cycle of mixed-layer depth (MLD) in GO5.0: (a) minimum monthly MLD in years 1996-2005; (b) minimum monthly MLD in the deBoyet Montégut et al climatology; (c) maximum monthly MLD in years 1996-2005; and (d) maximum monthly MLD in the deBoyet Montégut et al climatology. The hatching in panels a and b correspond to the areas of missing ocean data in panels c and d, where a full annual cycle of MLD is not observed in the de Boyer Montégut climatology.

2

(a)

(b)
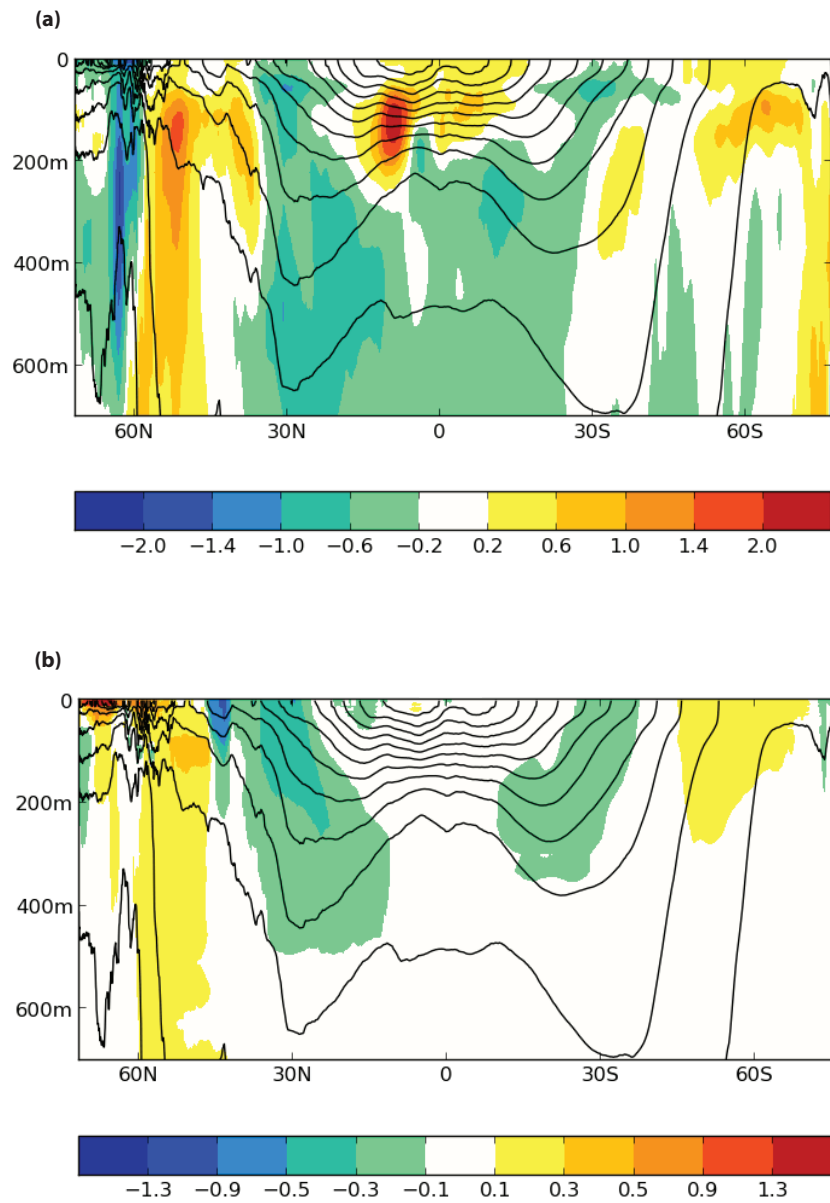
Figure 3. Zonal mean (a) temperature and (b) salinity biases in years 1996-2005 of GO5.0. The solid contours are of the zonal mean potential density σ_0, with a spacing of 0.5 kg m^3.

1

(a)

(b)
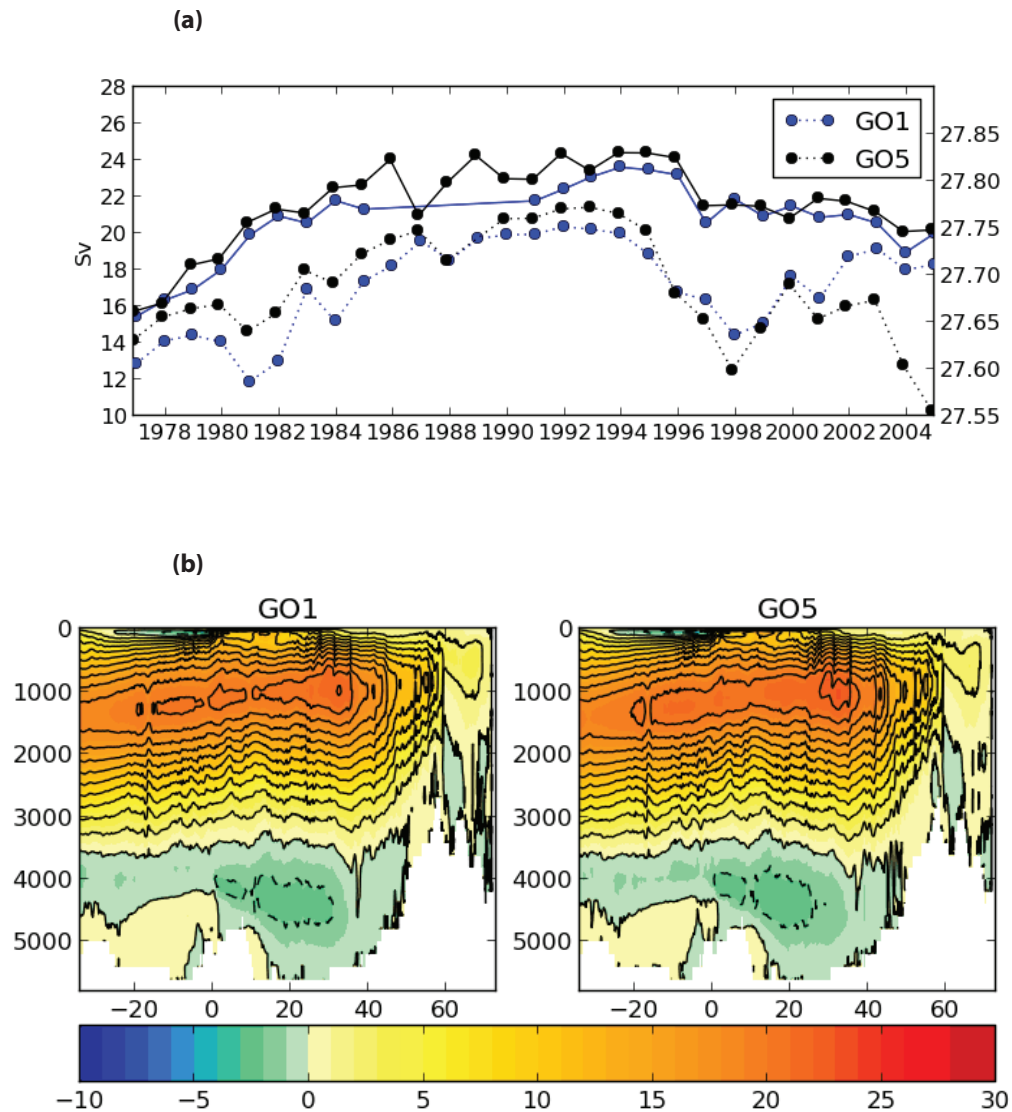
Figure 4. (a) Time series of the annual mean Atlantic meridional overturning circulation (AMOC) at 26°N in years 1996-2005 of GO1 and GO5.0, with the potential density σ_0 in the upper 200 metres in the central Labrador Sea; and (b) mean Atlantic overturning streamfunction in GO1 (left) and GO5.0 (right). Note that velocity data are missing in years 1986-1990 of GO1 .

1

(a)

(b)

(c)

(d)
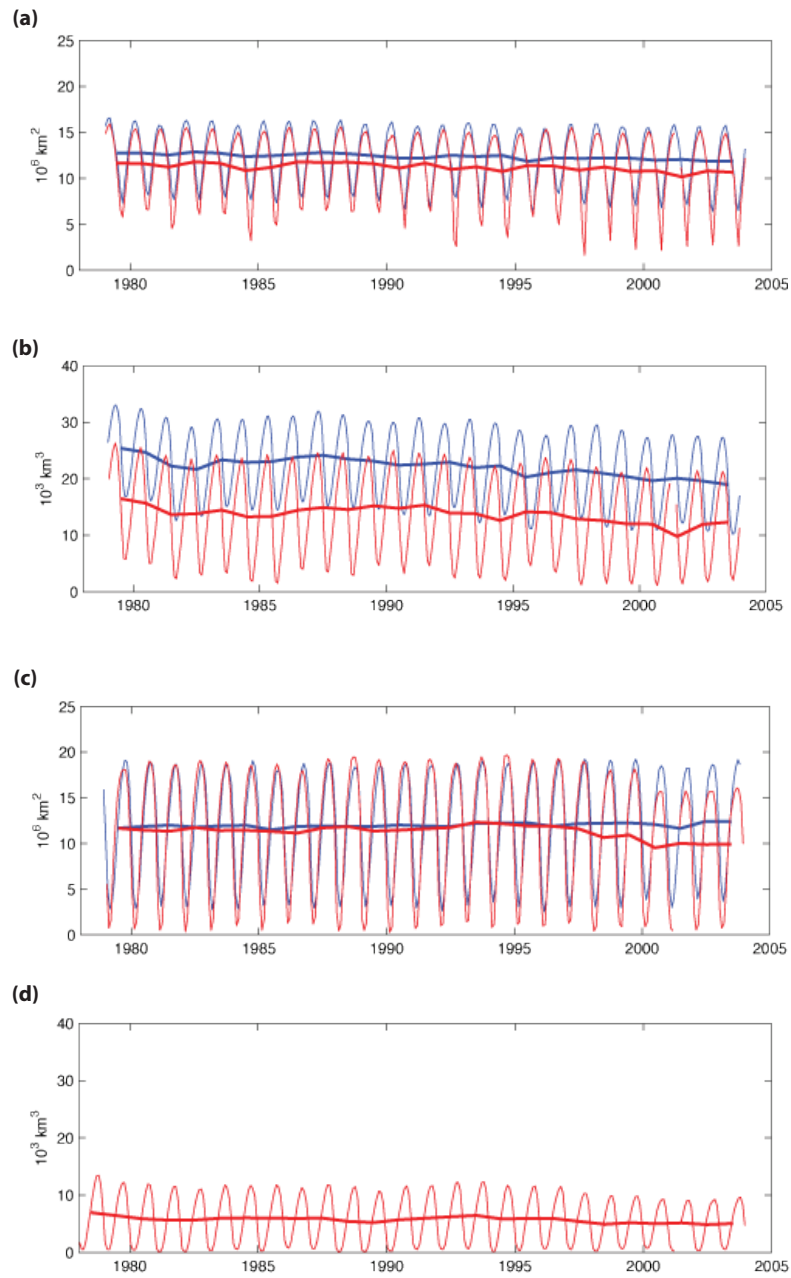
Figure 5 Time series of integrated sea ice properties in GO5.0 (red) and from observational estimates (blue): (a) Arctic mean ice extent; (b) Arctic mean ice volume; (c) Antarctic mean ice extent; and (d) Antarctic mean ice volume.

1
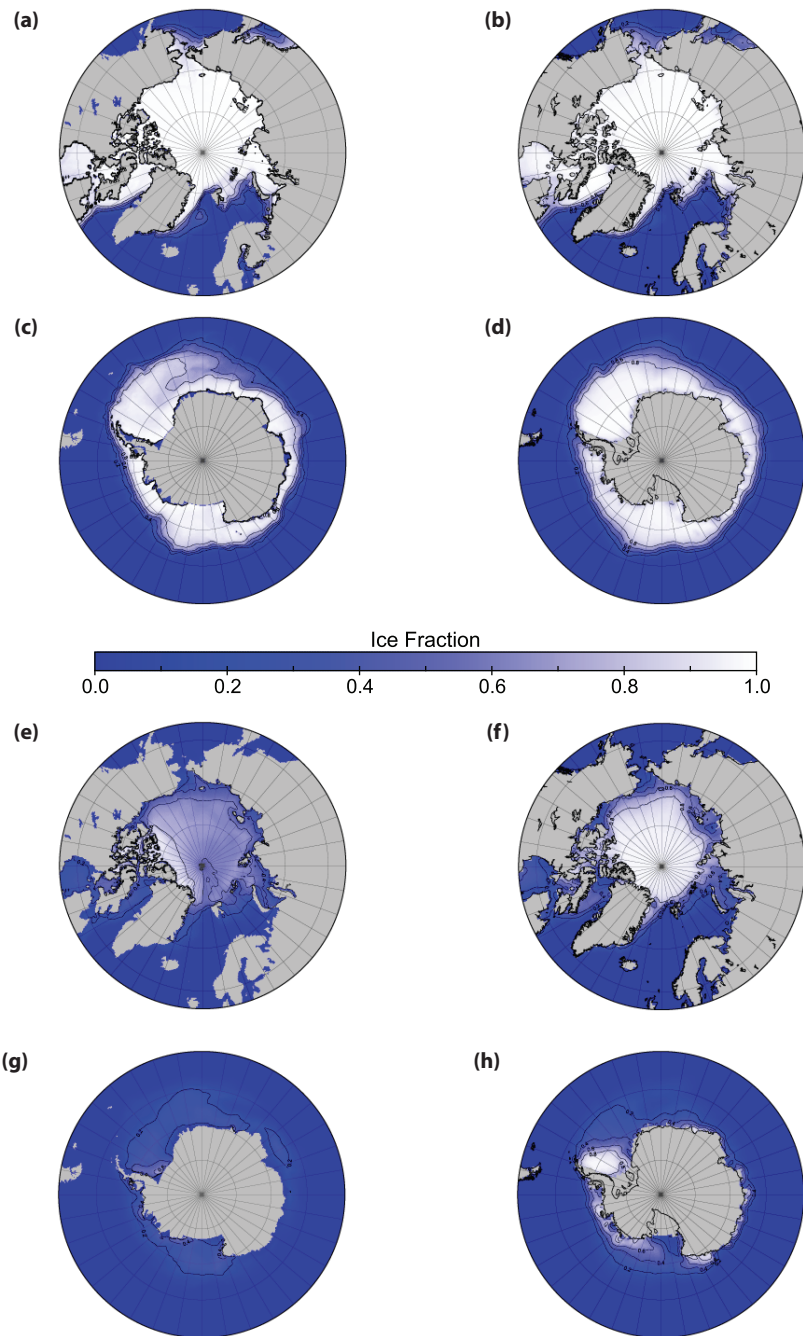
Figure 6 High-latitude sea ice extent in GO5.0 and in the HadISST observational dataset: Arctic winter (DJF) ice extent in (a) GO5.0 and (b) observations; Antarctic winter (JJA) ice extent in (c) GO5.0 and (d) observations; Arctic summer (JJA) ice extent in (e) GO5.0 and (f) observations; and Antarctic summer (DJF) ice extent in (g) GO5.0 and (h) observations.

1
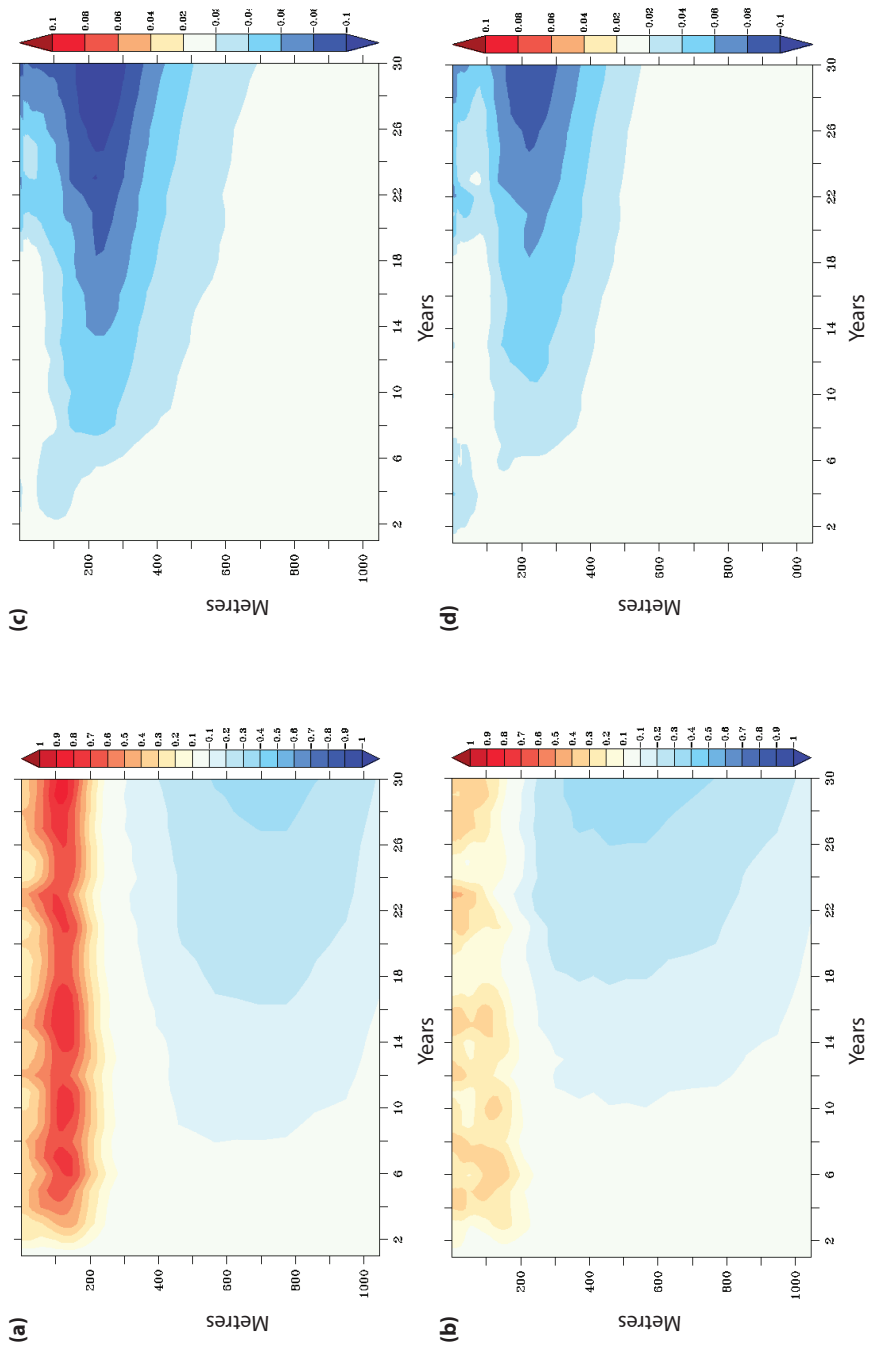
Figure 7. Subsurface drifts, defined as the difference of the horizontally-averaged annual mean in any year from that in the first year of integration, as a function of depth: (a) GO1 temperature drift; (b) GO5.0 temperature drift; (c) GO1 salinity drift; and (d) GO5.0 salinity drift.
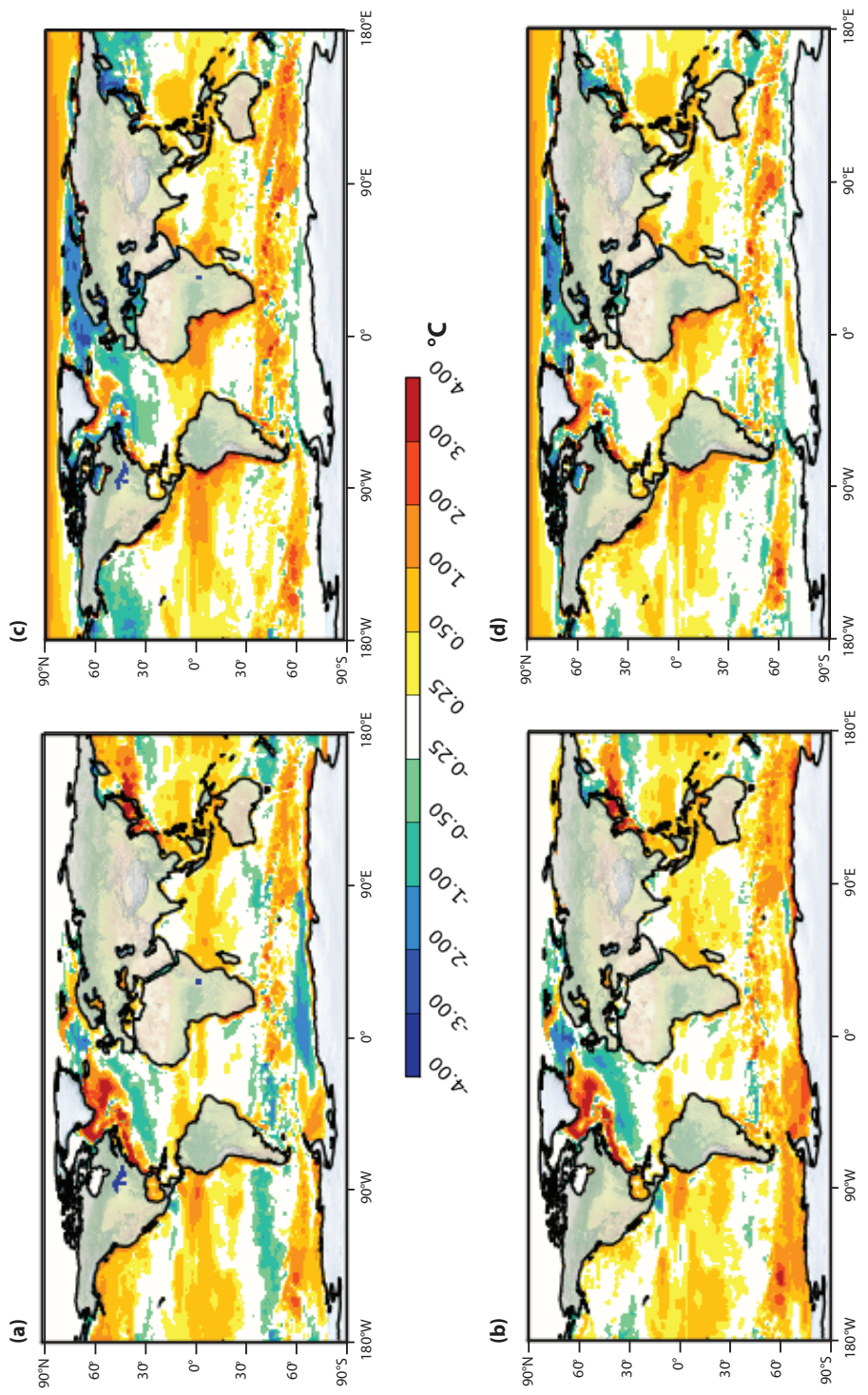
Figure 8. Seasonal sea surface temperature (SST) biases against Reynolds/Pathfinder climatology: boreal winter (DJF) biases in (a) GO1 and (b) GO5.0; and boreal summer (JJA) biases in (c) GO1 and (d) GO5.0.

1
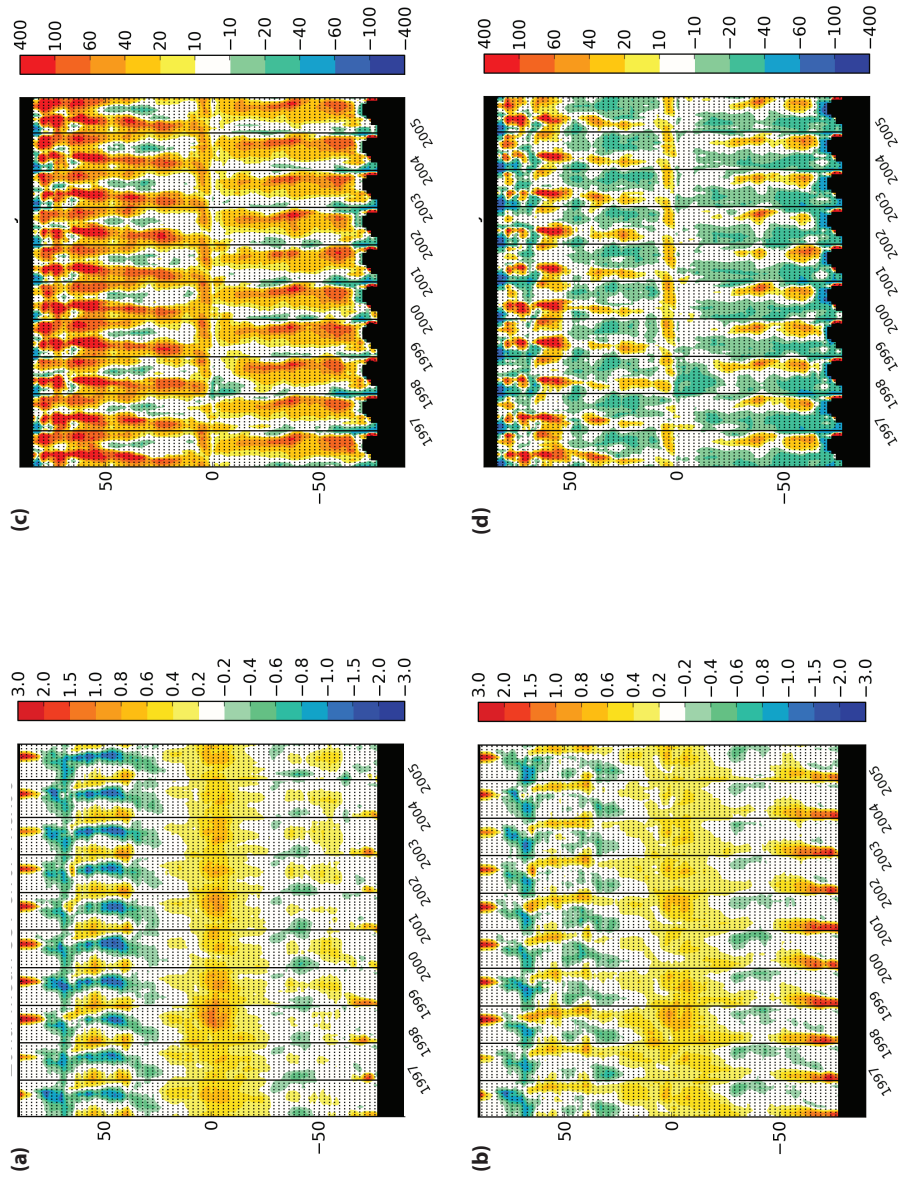
Figure 9 Monthly sea surface temperature (SST) and mixed layer depth (MLD) biases against Reynolds et al and de Boyet Montégut et al climatology, respectively, in years 1996-2005 as a function of latitude: (a) GO1 SST; (b) GO5.0 SST; (c) GO1 MLD; and (d GO5.0 (monthly) MLD.

1

1
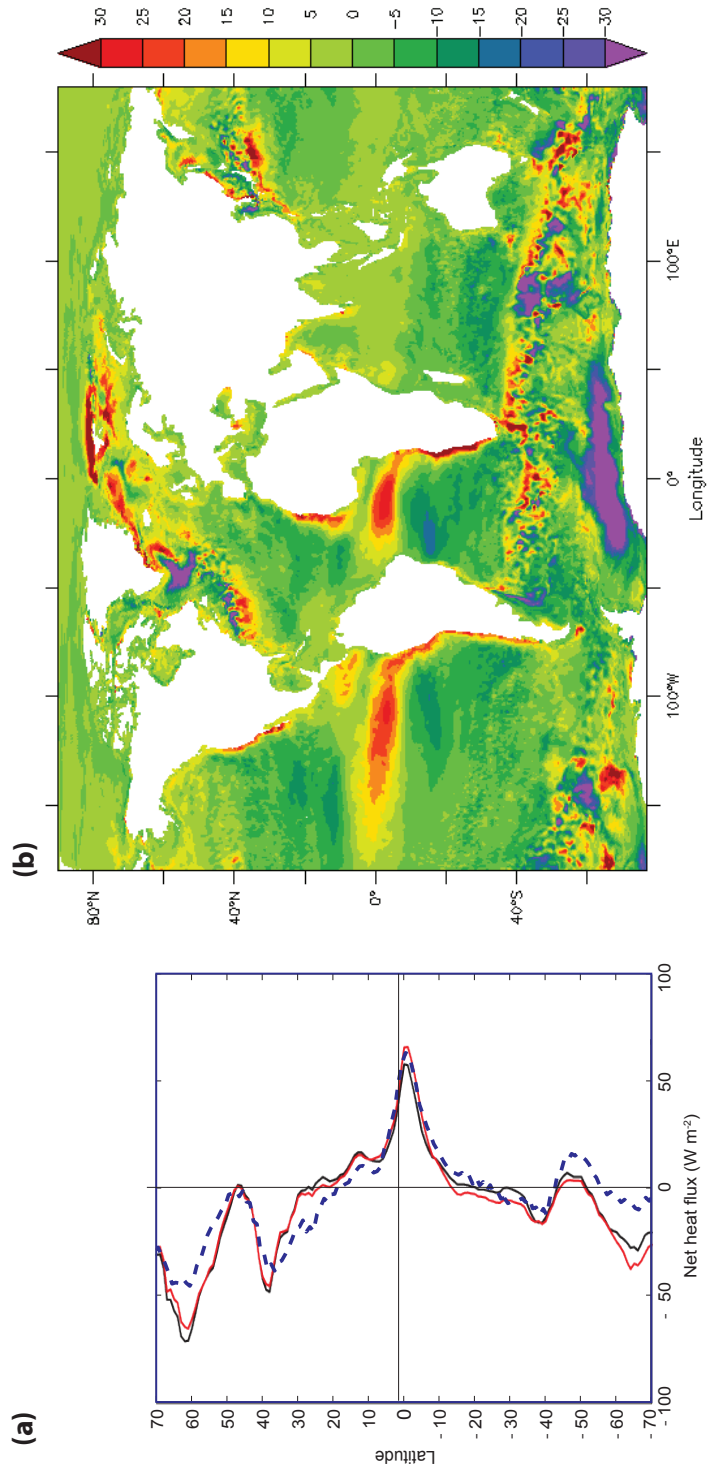
Figure 10. (a) Zonal mean net air–sea heat flux in GO1 (black); GO5.0 (red) and CORE2 data (dashed blue line) in years 1996-2005; and (b) surface net downward heat flux difference GO5.0 minus GO1.

2

63
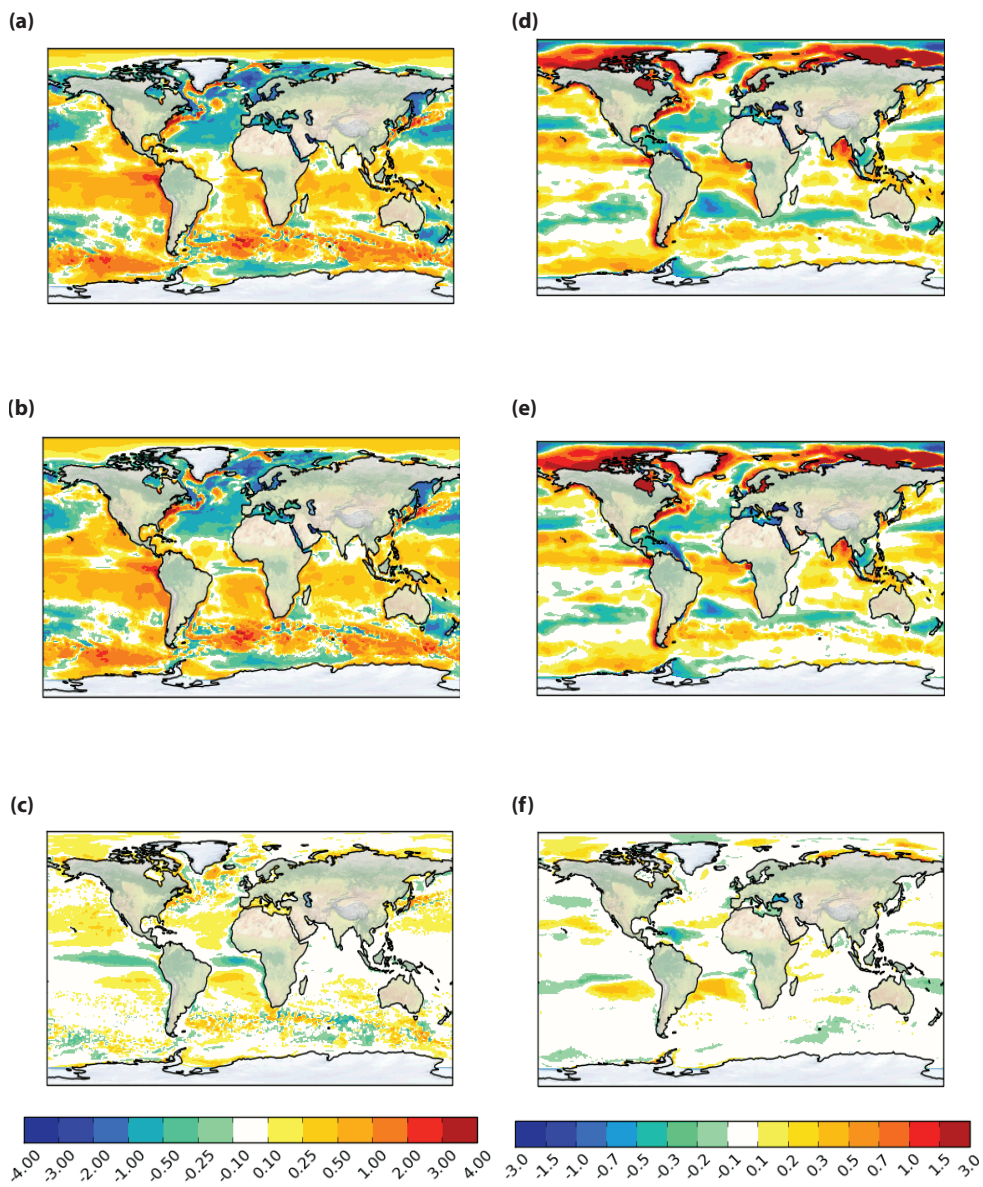
Figure 11 Effect on sea surface fields in years 1981-1985 of ocean code upgrade from v3.2 (GO1) to v3.4 (N3.4): (a) GO1 SST bias; (b) N3.4 SST bias; (c) N3.4 minus GO1 SST; (d) GO1 SSS bias; (e) N3.4 SSS bias; and (f) N3.4 minus GO1 SSS.

1
2
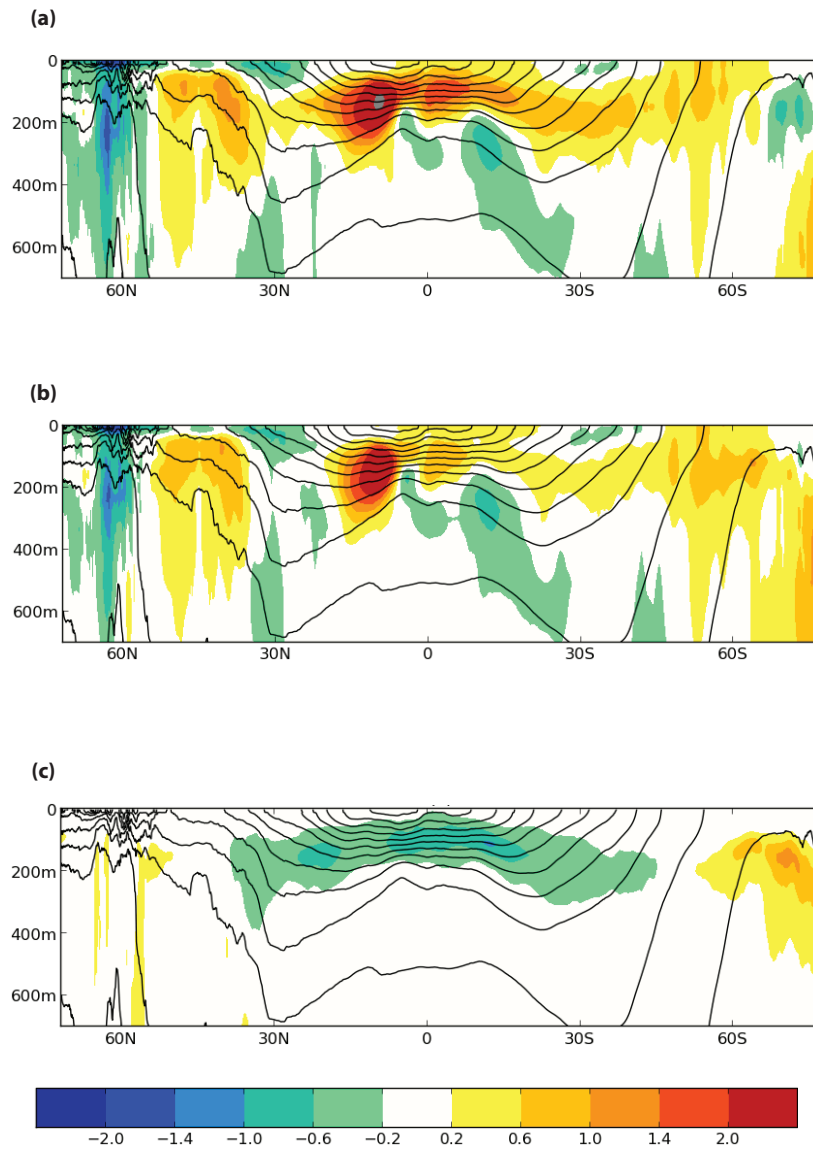
Figure 12. Effect on zonal mean temperature in years 1981-1985 of code upgrade from NEMO v3.2 (GO1) and v3.4 (experiment N3.4) in years 1981-1985: (a) bias in GO1; (b) bias in N3.4; and (c) difference N3.4 minus GO1. The black contours are of the mean isopycnals of the potential density σ_0 in N3.4 to show the position of the main pycnocline.
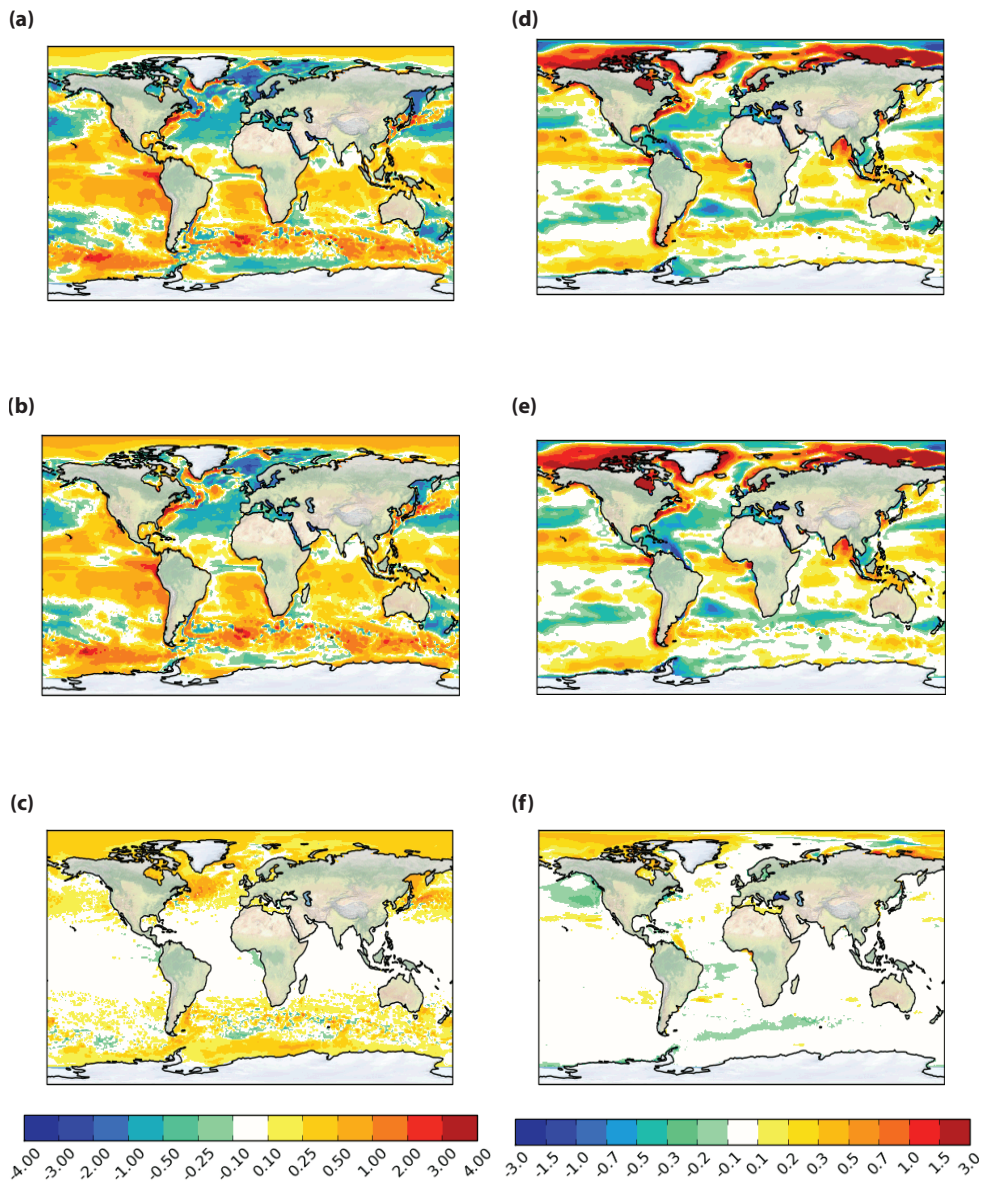
1

Figure 13 Effect on sea surface fields in years 1981-1985 of TKE scheme changes (from experiment N3.4_vmix to N3.4_tke): (a) N3.4_vmix SST bias; (b) N3.4_tke SST bias; (c) N3.4_tke minus N3.4_vmixSST; (d) N3.4_vmix SSS bias; (e) N3.4_tke SSS bias; and (f) N3.4_tke minus N3.4_vmix SSS.
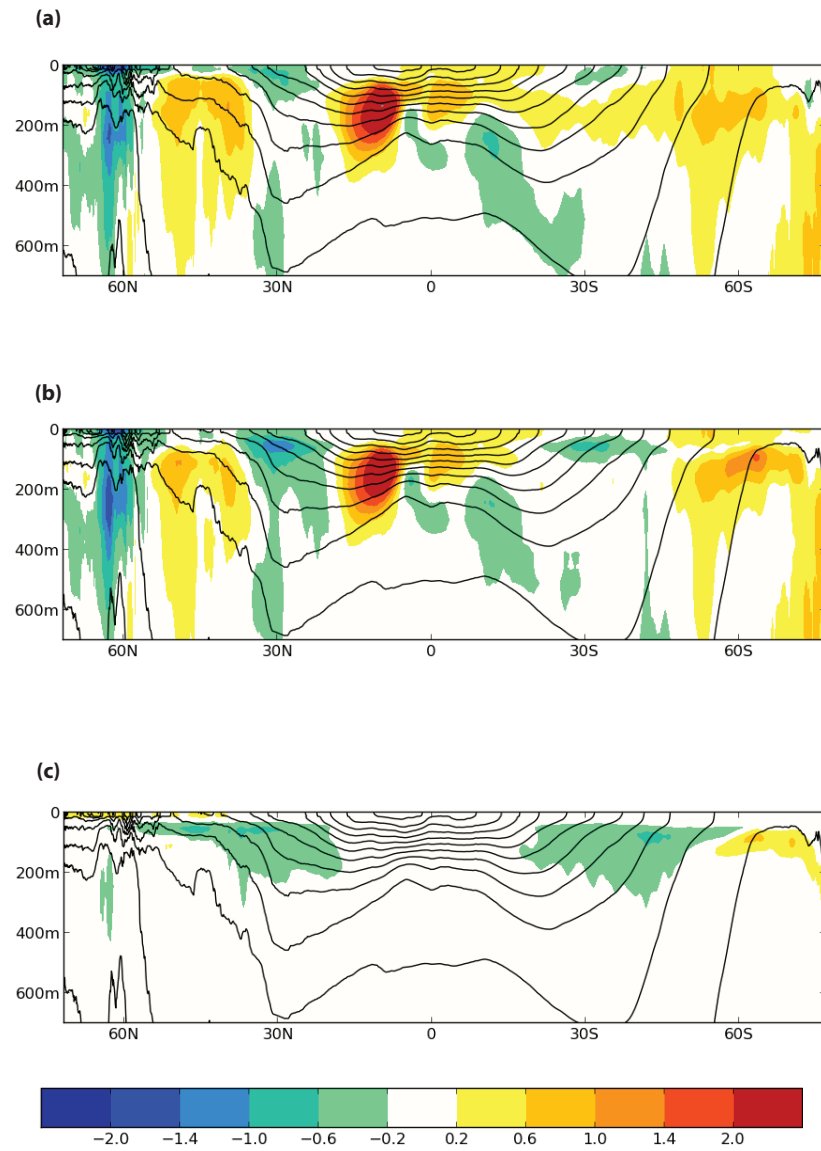
1

(a)

(b)

(c)

Figure 14. Effect on zonal mean temperature in years 1981-1985 of TKE scheme changes (from experiment N3.4_vmix to N3.4_tke): (a) bias in N3.4_vmix; (b) bias in N3.4_tke; and (c) difference N3.4_tke minus N3.4_vmix. The black contours are of the mean isopycnals of the potential density σ_0 in N3.4_tke to show the position of the main pycnocline.

1